THESIS FOR THE DEGREE OF LICENTIATE OF ENGINEERING

Comparative Study of different Recycling Methods for the Electrolyte Recovery from spent Li-Ion Batteries

NILS ZACHMANN

Department of Chemistry and Chemical Engineering

CHALMERS UNIVERSITY OF TECHNOLOGY

Gothenburg, Sweden 2023

Comparative Study of the different Recycling Methods for Electrolyte Recovery from spent Li-Ion Batteries
NILS ZACHMANN

Technical report no 2023:03

Department of Chemistry and Chemical Engineering
Chalmers University of Technology
SE-412 96 Gothenburg
Sweden
Telephone + 46 (0)31-772 1000

Cover: Illustration of the supercritical CO_2 extraction process set-up.

Chalmers Digitaltryck
Gothenburg, Sweden 2023

Comparative Study of different Recycling Methods for the Electrolyte Recovery from spent Li-Ion Batteries

NILS ZACHMANN

Industrial Materials Recycling
Department of Chemistry and Chemical Engineering
Chalmers University of Technology

Abstract

The state-of-the-art Li-Ion battery (LiB) recycling strategies focus mainly on recycling of the electrode materials, i.e., Li, Co, Mn, Ni, Al, and Cu. Thereby, the electrolyte, which is a multicomponent system consisting of a conductive salt dissolved in a mixture of organic carbonate solvents and additives, either evaporates and/or decomposes (uncontrollably). This causes a risk of immeasurable toxic and environmental emissions. Moreover, the remaining electrolyte in the produced black mass is problematic due to the presence of the organic solvents. Secondary streams coming from the recycling plants are then considered hazardous and represent a technical and financial burden for recycling companies.

As traditional methods fail to recycle the electrolyte from spent LiBs, it is evident that a new approach must be implemented to fill the gap. This work investigated two promising approaches to separate the electrolyte from spent LiBs; low temperature thermal treatment and sub-supercritical carbon dioxide ($scCO_2$) extraction. Thereby, the analysis emphasized the best possible process conditions to separate the electrolyte from spent LiBs, the composition and purity of the recovered products, and the composition of the exhaust gas emissions during the processes.

The results showed that the low temperature thermal treatment approach enables full separation and collection of the electrolyte solvents dimethyl carbonate (DMC), ethyl methyl carbonate (EMC), and ethylene carbonate (EC) after 80 minutes at 130ºC. However, the conductive salt $LiPF_6$ decomposed during the process leading to the generation of toxic exhaust gas emissions containing hydrogen fluoride (HF) and phosphorous oxyfluoride (POF_3). Sub-$scCO_2$ extraction with CO_2 densities between 600-900 kg/m^3 was suitable for selectively separating the non-polar electrolyte solvents DMC and EMC from the spent LiB in 30 minutes. The exhaust gas analysis and elemental analysis of the extracted product indicated that $LiPF_6$ did not decompose during the process but remained intact in the spent LiB. Thus, the sub-$scCO_2$ electrolyte extraction can be a promising toxic-emission-free approach for the selective extraction of the non-polar electrolyte solvents from spent LiBs. However, further investigation is required to extract the polar electrolyte solvents and $LiPF_6$.

Keywords: lithium-ion battery; electrolyte; recycling process; supercritical carbon dioxide extraction; thermal treatment; spectroscopy analysis; exhaust-gas emission characterization

List of Publications and Manuscripts

This thesis is based on the following publication and manuscript:

Paper I

N. Zachmann, M. Petranikova, B. Ebin, Electrolyte recovery from spent Lithium-Ion batteries using a low temperature thermal treatment process, *J. Ind. Eng. Chem. (2022). https://doi.org/10.1016/j.jiec.2022.11.020*

Contribution: Main author, all experimental work and data analysis.

Manuscript I

N. Zachmann, Robert V. Fox, M. Petranikova, B. Ebin, Implementation of a Sub-and Supercritical Carbon Dioxide process for the Selective Recycling of the Electrolyte Carbonate Solvents from Spent Li-Ion Battery, *(Submitted to Recources, Conservation and Recycling)*

Contribution: Main author, all experimental work and data analysis.

Abbreviations and Definitions.

The following abbreviations and definitions are used throughout this thesis.

Abbreviations.	Definition
%T	Percent Transmission
ATR	Attenuated Total Reflection
CO_2	Carbon Dioxide
DEC	Diethyl Carbonate
DMC	Dimethyl Carbonate
DMFP	Dimethyl Phosphorofluoridate
DTG	Differentiate Thermogravimetric
EC	Ethylene Carbonate
EMC	Ethyl Methyl Carbonate
EMFP	Ethyl Methyl Phosphorofluoridate
FTIR	Fourier-Transform Infrared Spectroscopy
GC-MS	Gas Chromatography coupled with Mass Spectroscopy
GWh	Gigawatt-hours
HF	Hydrogen Fluoride
HNO_3	Nitric Acid
IC	Ion Chromatography
ICP-OES	Inductively Coupled Plasma - Optical Emission Spectrometry
LiB	Lithium-Ion Battery
LiF	Lithium Fluoride
$LIPF_6$	Lithium Hexafluorophosphate
M	Molar
mmHg	Millimeter(s) of Mercury
N_2	Nitrogen
NMC	Lithium Nickel Manganese Cobalt Oxide
^oC	Degree Celsius
PAC	Protection Action Criteria
PF_5	Phosphorus Pentafluoride
PO_4^{3-}	Phosphate(3-) Ion
POF_3	Phosphoryl Fluoride/ Phosphorus Oxyfluoride
$scCO_2$	Supercritical Carbon Dioxide
SCF	Supercritical Fluid
TGA	Thermogravimetric Analysis
wt%	Weight Percentage
XRD	X-Ray Diffraction

Table of contents

1. Introduction

The first commercialized rechargeable Lithium Ion-battery (LiB) was released by Sony and Asahi Kasei in 1991. Since then, LiBs have been used in a variety of applications owing to the preferable combination of high energy and power density accompanied by a relatively long service life [1,2]. Devoted to these characteristics, the LiB became a key player in the shift towards electrically powered vehicles. Nowadays, the LiB is used in electrically powered vehicles, electrical storage systems and electrical portable consumer electronics (smartphones, laptops, tables, etc.).

Depending on the demand of the application, the LiB cell exists in four different shapes: cylindrical, prismatic, pouch and coin cell types. The LiB cell itself, regardless of its shape, is generally assembled from 5 different key components, i.e., the cathode, separator, anode, electrolyte, and case. When the cell case is opened, a layered structure of anode, separator and cathode can be observed, while the colorless electrolyte is embedded between those three. The nonaqueous electrolyte is a multicomponent system consisting of a conductive salt (mainly lithium hexafluorophosphate ($LiPF_6$)), organic carbonate solvents and additives. A combination of both non-polar and polar organic solvents is generally used for a high dissociation of the conductive salt, while achieving low viscosity. The layered cathode, anode and separator material form what is termed the electrode stack/jelly roll [3,4]. By electrically connecting a fixed number of LiB cells together with different battery management electronics inside a frame, a battery module is formed. In turn, a battery system, which is installed in an electrically powered vehicle, is composed of a fixed number of battery modules and various control/protection systems [3–5].

As a result of the excessive production and consumption of electric portable consumer electronics, electrical storage technology and electric powered vehicles, the demand for LiBs has steadily increased in the last few years. The sharp rise in LiB demand can be especially ascribed to the shift in the automotive industry toward electrically powered vehicles. The annual (automotive) Li-Ion battery demand increased from around 40 gigawatt-hours (GWh) in 2015 to 160 GWh in 2020, and more than doubled in 2021 to 340 GWh/year, whereas 1 GWh corresponds to approximately 5000 tons of materials considering a pack-level density of 200 Wh/kg [6,7]. In 2025, the total automotive LiB production amount is estimated to reach between 605 GWh/year to 1.6 TWh/year [8]. To meet this demand, several battery production sites are currently being constructed worldwide and plans for new Gigafactories are announced frequently. The expected electric vehicle battery life-time is about 10-15 years, whereas the LiBs in portable consumer electronics have a shorter anticipated life-time of 1.5-5 years, depending on the application [3,9]. Undoubtedly, a tremendous accumulation of end-of-life LiBs is to be expected in the coming years.

Developing environmentally efficient recycling processes for the treatment of the accumulated spent LiBs is essential for multiple reasons. Firstly, LiB is classified as hazardous waste and contains a variety of hazardous elements [10,11]. Unprocessed decomposition of end-of-life LiBs eventually leads to an enormous threat to the environment through leaching into the soil and groundwater. Moreover, the risk of fire scenarios of improperly stored spent LiBs is a proven concern. In the event of heating or fire a variety of toxic substances are released into the environment in the form of smoke and gases [12–15]. Secondly, recycling is an important source of raw material supply. In particular, lithium, cobalt, natural graphite and phosphorous

are listed as critical raw materials, which means that the raw material demand is forecast to overtake the supply in the near future [16]. The majority of the (critical) LiB raw materials are mined and produced outside of Europe, in countries such as DR Congo, China, Chile, Russia, South Africa, and Australia [17]. Without an efficient recycling strategy, the EU is highly dependent on its geopolitical relations to realise the full electrification of transportation anticipated by 2035 [18]. Most importantly, the recycling and treatment of end-of-life LiBs is mandatory and has been regulated by an EU directive since 2006 [19]. In 2019 the EU directive was adjusted, and the new proposal imposes a total LiB recycling efficiency by weight of 70% by 2030 [20,21].

The current industrialized and lab-scale LiB recycling processes focus mainly on the development and research of the recovery of the valuable cathode active material metals (Li, Co, Mn, Ni), and the current collector materials (Al, Cu) [3,9,22]. Thereby, the recovery of the electrolyte has received little attention, and electrolyte treatment details are often ignored. The electrolyte is challenging to reutilize due to its volatile nature and the thermal instability of the conductive salt, lithium hexafluorophosphate ($LiPF_6$). During the state-of-the-art recycling strategies, the electrolyte components are prone to evaporate uncontrollably and decompose [23–25]. The resulting hazardous gas emissions are then considered to be a threat for the work environment in the recycling plants and to the environment. The release of small electrolyte amounts can quickly form a concentrated toxic atmosphere, reaching an acute exposure limit such as the protection action criteria (PAC) 2, where irreversible and other serious health effects are very likely [11]. Undoubtedly, an environmentally efficient strategy to fully recycle the electrolyte from end-of-life LiB is required to minimize the impact of battery recycling on the environment and to improve work safety in the recycling plants.

As the state-of-the-art recycling processes fail to fully recycle the electrolyte from the spent LiBs, an alternative approach must be developed and implemented. The most promising options for the recovery of the electrolyte are vacuum distillation, low-temperature thermal treatment, organic solvent extraction or sub- and supercritical carbon dioxide ($scCO_2$) [9,26,27]. Extended research on these approaches is still limited, and further research is required for a proper understanding of the impact of the different process parameters on the composition and purity of the recovered electrolyte and the process exhaust gas emissions. In this thesis two different approaches to recover the electrolyte from spent LiBs for an EV application were studied and compared. These approaches were low temperature thermal treatment and sub- and $scCO_2$ extraction. Thereby, the analysis of the composition and purity of the collected separated products, the process exhaust gas emissions composition, and the impact of the processes on the active cathode material was emphasized.

2. Background

2.1. EU Directive for Batteries and Waste Batteries

The Batteries Directive (2006/66/EC) has regulated batteries and waste batteries at the EU level since 2006 [19]. A new proposal to modernize the legislation by the European Commission was proposed in 2020 and was accepted by the European Parliament and Council in 2022 [20,21]. The proposal is closely linked to the European Green Deal and the Circular Economy Action Plan. A modernization of the legislation was essential to react to the technological and socioeconomic development, as well as the future challenges in the battery sector. The new proposal addresses the social, economic, and environmental impact of all types of batteries sold and produced within the EU and covers the entire battery life cycle, from design to production to their end-of-life treatment. The overall aim is to promote competitive sustainability in Europe to boost the circular economy of the battery value chain, to provide legal certainty, to increase the transparency of the battery market, as well as the traceability of large batteries throughout their life cycle, and to minimize their environmental impact by promoting more efficient use resources.

Among other regulations in the design, production and traceability of batteries, the new legislation defines requirements and targets for the collection, recycling, and treatment of spent batteries. The responsibility to finance the collection, treatment and recycling of disposed batteries is put on the battery producer. The collection target for spent portable batteries was set to 65% by 2025 and 70% by 2030. Batteries intended for use for light means of transport, automotive, industrial and EV are excluded from the collection target, but a full collection is anticipated for the latter. The overall LiB recycling efficiency by average weight was declared to reach at least 65wt% by 2025 and 70wt% by 2030. The defined specific material recovery targets are Co (95%), Ni (95%), Li (70%) and Cu (95%) by the end of 2030. A requirement on the treatment states that it must include, as a minimum, the removal of all fluids and acids.

2.2. Lithium-Ion Battery Components and their Composition

A battery system (pack) installed in an electrically powered vehicle is composed of a fixed number of battery modules and various control/protection systems. The battery module is formed by electrically connecting a fixed number of LiB cells together with different battery management electronics placed inside a frame. The Li-Ion battery cell exists in four different shapes, cylindrical, prismatic, pouch and coin cell [3–5].

A standard LiB cell, regardless of its shape, is assembled from 5 different key components; the cathode (20-35wt%), separator (4-10wt%), anode (15-25wt%), electrolyte (10-20wt%), and the case (4-20wt%) [5,28]. The cathode, anode and separator material are layered and form what is termed the electrode stack/jelly roll. The electrode stack/jelly role is inserted in a cover. Finally, the non-aqueous liquid electrolyte is injected into the assembly, and the cover/shell is hermetically sealed [3].

2.2.1. Cathode

The cathode, the positive electrode, is composed of a current collector, the active cathode material and a binder. The polymeric binder coats the active cathode material attached to the current collector and enhances the adhesion between them. Several different chemical

compositions of the active cathode material are currently on the market and new chemistries are continually evolving. The most common and commercialized active cathode chemistries are composed of different transition metals and are the name-giver of the LiB cell; Lithium Nickel Cobalt Manganese Oxide (NMC), Lithium Iron Phosphate (LFP), Lithium Nickel Manganese Spinel (LMNO), Lithium Nickel Cobalt Aluminum Oxide (NCA), Lithium Manganese Oxide (LMO), and Lithium Cobalt Oxide (LCO). Thin aluminum foils are mainly used as the current collector material. The state-of-the-art polymeric binder material is polyvinyl fluoride (PVDF) [1,3–5].

2.2.2. Anode

The anode, the negative electrode, is composed of a current collector (thin copper foil), the active anode material and a binder. Natural, high-grade graphite is the most used active anode material, but lithium titanium oxide ($Li_4Ti_5O_{12}$) is also common. Commercialized anode binder materials are carboxymethyl cellulose (CMC), styrene butadiene rubber (SBR) or PVDF [1,4,5].

2.2.3. Separator

The separator prevents contact between the anode and the cathode while maintaining high permeability to the conductive salt. Polyolefins such as polypropylene (PP) and polyethylene (PE) are the main components of the state-of-the-art separator. Additionally, the separator membrane can be ceramic or PVDF [30].

2.2.4. Electrolyte

The electrolyte is the indispensable ionic conductor between the cathode and the anode and is responsible for the smooth cation and anion transfer during the LiB charging and discharging process [31]. In general, three families of LiB electrolytes exist, i.e., liquid, polymer and solid electrolytes, and several different electrolyte chemistries have been developed [32]. New electrolyte formulations will continue to evolve with the constant development of new battery chemistries [33]. The state-of-the-art LiB electrolyte is the non-aqueous liquid electrolyte, which is a multi-component system composed of a conductive lithium salt, electrolyte solvents and additives [34]. The total amount and exact composition of the electrolyte in the LiB cell is often unknown and varies from producer to producer. Generally, the total amount of electrolyte is between 10-20wt% of the LiB cell [5,28]. The largest proportion of the non-aqueous liquid electrolyte is generally the electrolyte solvent, whether by volume, weight, or mole fraction, whereas the additives typically amount to up to 5% - (either by weight or by volume) - of the total composition [35]. The conductive salt is dissolved in an organic electrolyte solvent mixture. Lithium hexafluorophosphate ($LiPF_6$) is the most used conductive salt not because of any outstanding property but rather due to the lack of any significant disadvantage. However, other lithium salts such as borates ($LiBF_4$, LiBOB, LiDFOB), sulfonylimides (LiTFSI, LiFSI, LiBETI) or lithium perchlorate ($LiClO_4$) are possible replacements [35,36]. The most favored electrolyte solvent used is the high-dielectric-constant cyclic carbonate ethylene carbonate (EC), which enables strong lithium-salt dissociation and has a unique ability to form a stable protective layer on the cathode interphase. To improve the conductivity by lowering the high viscosity of EC (solid at room temperature), a mixture of linear alkyl carbonates such as dimethyl carbonate (DMC), ethyl methyl carbonate (EMC) and diethyl carbonate (DEC) are generally used [31,32,34,35]. A wide range of additives can be added to the electrolyte solvent mixture to address different challenges, i.e., improvement of the flammability, enabling overcharge protection, enhancement of conductivity, and pushing the electrolyte to optimized

battery operation [32,35]. Common additives are vinyl carbonate (VC), fluoroethylene carbonate (FEC) or tris(trimethylsilyl)phosphite (TMSPi). An overview of the most common components in the state-of-the-art non-aqueous electrolytes including their chemical and physical properties as well as hazard identification based on the Classification, Labelling and Packaging Regulation (Regulation (EC) No. 1272/2008) is shown in Table 1 [11,34,37].

Table 1. Summary of the most common non-aqueous electrolyte components including their structure, melting point (T_m), boiling point (T_b), vapor pressure (p_v), dielectric constant (ε), dipole moment, and hazard identification.

Compound	Structure	T_m [°C]	T_b [°C]	p_v[a] [mmHg]	ε [25°C]	Dipole Moment [D]	Hazard
Dimethyl Carbonate (DMC)	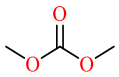	4	90	55.36	3.1	0.76	
Ethyl Methyl Carbonate (EMC)	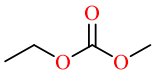	-55	110	32	2.9	0.89	
Diethyl Carbonate (DEC)	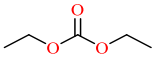	-74	129	11.5	2.8	0.97	
Ethylene Carbonate (EC)	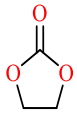	36.5	248	0.0098	89.8	4.61	
Propylene Carbonate (PC)	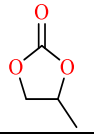	-49	242	0.045	64.9	4.81	
Lithium Hexafluorophosphate ($LiPF_6$)	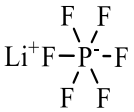	N/A	N/A	N/A	N/A	N/A	

[a] Vapor pressure at 25°C. The vapor pressure of water is 23.8 mmHg at 25°C.

2.2.5. Case

The hermetically sealed case protects the electrode stack from the environment. The case material varies depending on the shape of the LiB cell and can be made of metal foil, steel, aluminum or plastic.

2.3. State-of-the-art LiB Recycling Strategies

The state-of-the-art LiB recycling strategies include either pyro- or hydrometallurgy processes or a combination of both [3,9,22]. In the pyrometallurgy processes, high temperature furnaces are used to smelt/roast/calcinate the entire LiB cells or modules to form an alloy of Co, Cu, Fe and, Ni. Chemical processing is generally used to separate the metals from the alloy into the particular metals. Besides the metallic alloy, slag and gases are produced during the process. The metals in the formed slag (Al, Mn, Li) are challenging to recover in hydrometallurgical processes and are usually sold to other industries. An advantage of pyrometallurgy treatment is that dissembling, discharging, or pre-treatment of the LiB cell is not required. However, toxic and environmentally harmful gases are formed while the separator, binder material, electrolyte and graphite evaporates, decomposes, or gets burnt off at high temperatures [3,9].

The hydrometallurgy process includes a pre-treatment step that includes dismantling, sorting, crushing, shredding, grinding, and milling to produce a black mass. The black mass is a mixture of cathode and anode material. The transition metals (Li, Co, Mn, Ni) in the black mass are conventionally recovered by leaching, solvent extraction, ion exchange, crystallization and/or filtration processes. Often a thermal pre-treatment step (pyrolysis, incineration or calcination) is used to deactivate, liberate and reduce the active materials at elevated temperatures above 550ºC. During this step, the binder material, separator and electrolyte decompose, while forming toxic and environmentally harmful gas emissions and are lost for reutilization [3,9,10,22]. Moreover, during the mechanical pre-treatment process, the volatile electrolyte components are prone to evaporate [23–25].

2.4. The Fate of the (non-aqueous) Electrolyte in State-of-the-Art LiB Recycling Processes

The current industrialized and lab-scale recycling processes focus mainly on the recycling of the valuable cathode active material transition metals (Li, Co, Mn, Ni), and the current collector materials (Al, Cu) [3,9,22]. The recovery and recycling of the electrolyte receives little attention, and electrolyte treatment details are often ignored. In the pyrometallurgical processes the spent batteries are smelted, whereby the electrolyte components vaporize, decompose, or are disregarded in the slag [3,9]. In hydrometallurgical recycling processes, several pre-treatment steps are generally required for the efficient recovery of the cathode's active materials. A black mass containing cathode and anode material is generated by dismantling, sorting, separation, crushing, shredding, grinding, and milling of the spent LiBs. Thermal pre-treatment at high temperatures (<550ºC) is additionally preferred to liberate the cathode's active material from the current collector and for calcination of the black mass [3,9,10,22]. During the common pre-treatment steps in the hydrometallurgical process, the electrolyte components either decompose and/or evaporate causing a risk of immeasurable environmental and toxic emissions [23–25].

The electrolyte solvents currently used today are (very) volatile and inflammable and the conductive salt, $LiPF_6$, is known to be thermally unstable and prone to decompose to the highly

toxic hydrogen fluoride (HF), phosphorus pentafluoride (PF_5) and phosphorus oxyfluoride (POF_3) [10,11,25,38–43]. For HF especially, the inhalation toxicity threshold is already reached at levels of just a few ppm. The release of small electrolyte amounts can quickly form a concentrated toxic atmosphere reaching an acute exposure limit such as protection action criteria 2, where irreversible and other serious health effects are very likely [11]. Undoubtly, inappropriate handling and treatment of the electrolyte from the LiB waste, resulting in exposure, has a tremendous impact on the work environment in the recycling plants and on the environment. A LiB cell consists of 10-20wt% of electrolyte, depending on the shape and chemistry [28]. Consequentially, by ignoring the recycling of the electrolyte, a major part of the potentially recyclable and reusable LiB waste material is lost [44].

2.5. Processes to Recycle the Electrolyte from spent LiBs

A few research groups have dedicated their research towards the recycling of the electrolyte from spent LiBs. The most promising techniques are vaporization processes, organic solvent extraction and sub-supercritical CO_2 technology [15,26,45,46].

2.5.1. Vaporization Processes

Vaporization refers to the transition of the physical state of a substance into the vapor phase. Sufficient kinetic energy is required to overcome the intra-molecular forces of the substance for its change into the vapor phase. The amount of energy/temperature required to induce the phase change is determined by the boiling point of the substance. Below the boiling point, the vaporization process is typically called evaporation. The rate at which a substance evaporates is dependent on its vapor pressure and the temperature. The higher the vapor pressure and/or temperature, the faster the substance tends to evaporate. The vapor pressure of a substance can also be significantly increased by lowering the surrounding pressure of the substance. The concept of thermal vaporization has been applied to recycle the electrolyte from spent LiB. Zhong et al. [46] used low temperature volatilization at 120°C to recycle the electrolyte without any specification of the (reclaimed) electrolyte composition or analysis of the resulting exhaust gas emission. Stehmann et al., [47] implemented a vaporization process to thermally dry shredded LiBs at low pressure (<300mbar) to recover the electrolyte. The recycling company Duesenfeld report recovery of the electrolyte from spent LiBs by using vacuum vaporization [48].

2.5.2. Organic Solvent Extraction

In the organic solvent extraction approach, the LiB electrode and separator waste is immersed into an organic extraction solvent to eventually dissolve the electrolyte. The electrolyte, in turn, is separated from the extraction solvent by distillation based on the different boiling points of the electrolyte components [49]. He et al., [50] reported an electrolyte extraction yield of 95.6% (PC, EC, $LiPF_6$) using a complex aqueous peeling agent made in-house, namely exfoliating and extracting solution (AEES). Thereby, the conductive salt $LiPF_6$ was converted into $NaPF_6$ and Li salt in the extraction process. Zhu et al., [51] completely dissolved the electrolyte in a DMC solution after 24 hours and applied subsequent processing steps to downgrade $LiPF_6$ to calcium fluoride (CaF_2) from the $LiPF_6$. Haas et al., [52] used a combination of DMC and H_2O in a multi-stage-cross-flow extraction system to successfully reduce the sample fluoride content in lab scale experiments while extracting EC, DMC and EMC from end-of-life LiBs.

2.5.3. Supercritical Fluid Extraction

Chemical industry processes often rely on volatile, toxic, flammable, hazardous organic environmentally damaging solvents [53]. A potential solution to make chemical industrial processes more environmentally efficient is the so-called Green Chemistry. Anastas and John Warner developed the "Twelve Principles" of Green Chemistry to define its main goals and realizations in practice [54]. Supercritical fluids (SCF) fulfil these Green Chemistry goals and have been attracting scientific and industrial interests over the past few decades due to their huge potential. SCF technology is already heavily employed in the pharmaceutical, cosmetic, beverage, dyeing, and food industry [55].

Among the SCFs, supercritical carbon dioxide has been attracting special interest because it is non-toxic, non-flammable, abundant, cheap, recyclable, unrestricted by the Environmental protection agency, and is easily achieved under mild conditions. $ScCO_2$ is formed once the pressure and temperature of CO_2 exceed its critical temperature (T_c) of 31°C and critical pressure (P_c) of 73.8 bar illustrated in Figure 1 [53,56].

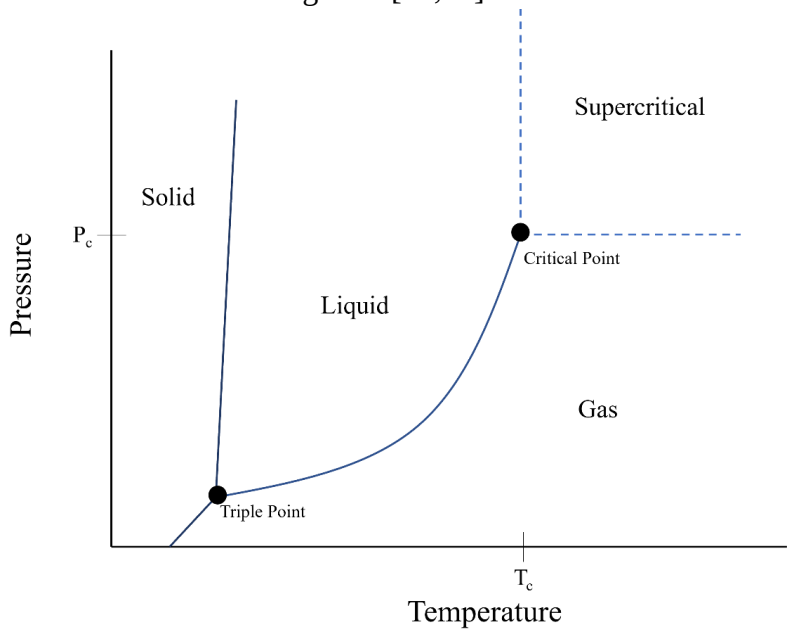

Figure 1. Illustration of the pressure-temperature phase diagram of CO_2.

In the so-called supercritical state, CO_2 obtains superior physicochemical properties such as liquid-like densities, gas-like compressibility and viscosity diffusion coefficient and negligible surface tension. Those properties can be easily fine-tuned under the variation of temperature and pressure conditions. As a result, the $scCO_2$ technology is advantageous compared to the use of conventional extraction processes because of its excellent mass transfer characteristics, i.e., the quick spread of the solvent, the possibility to penetrate into the solute matrix, fast dissolution times and easy removal from the products by depressurization [57,58]. After the extraction, CO_2 can then be recycled back to the process.

The sub-and $scCO_2$ extraction technology is predestined to recover the electrolyte due to its outstanding features, i.e., excellent mass-transfer characteristics, non-flammability and environmentally friendly “infinite reusability of CO_2”, decreasing consumed solvent amount and low reactant and processing costs. Electrolyte separation by sub- and $scCO_2$ technology from LiB separator material and spent 18650 LiBs has been investigated in a few studies at

various pressure and temperature conditions [59–66]. According to the literature, the extraction yields of the different electrolyte solvents (DMC, EMC, DEC, EC, and PC) and the conductive salt ($LiPF_6$) are sensitive to the process conditions pressure, temperature and the extraction mode (static and follow-through extraction). A combination of static and flow-through extraction was reported to be beneficial for a high electrolyte extraction yield [60]. Variations in pressure (150-350 bar) and temperature (30-50 ºC) caused a similar trend for the extraction of the non-polar linear carbonates DMC and EMC, which was attributed to their similarity in structure and polarity [62]. It was reported that the electrolyte extraction efficiency of spent LiBs was almost doubled using an additional co-solvent compared to pure liquid (60 bar, 25ºC) and supercritical (300 bar, 40ºC) CO_2 extraction while DMC, EMC were quantitatively recovered and the polar components EC and $LiPF_6$ qualitatively recovered [60].

2.6. Challenges in the Recycling of Electrolyte

The electrolyte in aged LiBs is prone to penetrate and diffuse into the pores of the electrode structure, and after long-term electrochemical operation eventually immobilizes [26,27]. Moreover, the electrolyte composition and total amount in the battery cell are unknown, inhomogeneous and can vary from producer to producer [26,33]. This and the special physical and chemical properties of the electrolyte mixture components, i.e., (very) volatile, inflammable, thermally unstable, and hazardous, complicates the electrolyte recycling design [10,11]. However, despite its low economical value compared to the valuable transition metals, the safe removal of the electrolyte is essential from an environmental point of view, since this reduces the greenhouse gas emissions generated by the incineration of the electrolyte and reduces the threats associated with the LiB waste, while the safety of the overall recycling process also increases [67].

The electrolyte solvents commonly used in the electrolyte mixture are (very) volatile and prone to instantly evaporate at room temperature as soon as the battery cell is opened. In particular, the most common electrolyte solvents DMC and EMC are highly volatile with vapor pressures of 55 mmHg and 32 mmHg at 25ºC. The release of only a small amount of electrolyte can create a toxic atmosphere, with concentrations of the released compound reaching an acute exposure limit for the workers in the recycling plant. DMC, for instance, reaches the PAC-1 level at concentrations of 39 mg/m^3, PAC-2 at 430 mg/m^3 and PAC-3 level at 2600 mg/m^3 [11]. Moreover, the flammable nature of the electrolyte solvents can cause adverse reactions leading to fire or explosions in the recycling plants [68].

Another challenge is the poor thermal stability and sensitivity towards moisture of the most common conductive salt, $LiPF_6$. The decomposition pathway includes the generation of the toxic gases HF, PF_5 and POF_3. Besides being a major safety concern, the $LiPF_6$ decomposition products eventually react with the electrolyte solvents to form various aging products during the LiB cycling life, or potentially in the electrolyte recycling process, which reduces the purity of the reclaimed product [27,64,67,69,70]. A variety of organophosphate-based and organic fluorophosphate-based products were reported in aged LiB, including dimethyl phosphorofluoridate (DMFP), ethyl methyl phosphorofluoridate (EMFP) and diethyl phosphorofluoridate (DEFP). PF_5 is also known to enhance the transesterification of the carbonate solvent. For instance, in the presence of PF_5, the transesterification products DMC and DEC are formed from the decomposition of EMC. Consequently, the reclaimed product eventually requires purification before its reutilization.

3. Theory

3.1. Solvation Characteristics of Supercritical Carbon Dioxide

The CO_2 molecule is linear and centrosymmetric and consequently has a zero net dipole moment. Thus, $scCO_2$ is generally classified as a non-dipolar solvent, being a good solvent for many non-polar low-molecular-weight compounds. CO_2 possesses a significant quadrupole moment generated by its bond dipoles. It is well-established in the literature that CO_2 can act as both a weak Lewis acid or base and can participate in conventional and nonconventional hydrogen-bonding interactions [53,71,72]. In $scCO_2$ extraction the solvation characteristics are highly related to the density. As the mean molecular distance decreases with increasing densities, the specific solute and solvent interaction probability increases proportionally. The CO_2 density can be adjusted by variation of pressure and temperature. At a constant temperature, the CO_2 density increases with increase of pressure. Thus, the solvation power increases. The effect of the temperature is more complex, especially in solid phase solutes, since several competing factors play a role such as the solvent density, solute vapor pressure and kinetics. At a given pressure, the solute vapor pressure and kinetics increase with temperature, but meanwhile the solvent density decreases and so does the probability of the solute-solvent interactions. The competing effects can be differentiated by what is termed the cross-over effect. Below the cross-over pressure, the density effect dominates, and the solvation power of CO_2 decreases with temperature increase at a constant pressure. However, above the cross-over pressure, the $scCO_2$ density changes are not remarkably significant any longer and the vapour pressure and kinetic effects become dominant. Thus, at a constant pressure the solvation power increases with temperature [58,73].

Under readily achievable pressure and temperature conditions, however, CO_2 is an ineffective solvent for high molecular weight polymers and ionic compounds of high polarity. Nevertheless, the solubility properties of CO_2 can be significantly improved by adding a co-solvent/modifier [58,74–76]. Thereby, the role of $scCO_2$ is believed to be limited by providing the supercritical phase, whereas the modifier-solute interactions is responsible for the solubility increases of the polar compounds [75,77].

$ScCO_2$ extraction is typically achieved in static and/or dynamic modes. In the dynamic (flow-through) extraction mode, a constant CO_2 flow is applied throughout the entire extraction time while keeping the pressure and temperature conditions constant. In the static extraction mode, the pressure and the temperature are kept constant without a flow of CO_2 and CO_2 is released from the reactor after the extraction time. The dynamic mode is favoured when the solvent and solute reach the equilibrium fast [58,78]. The extracted species can then be separated from the CO_2 solvent by depressurization or by changing the temperature. The most common techniques are solvent bubbling, collection on a sorbent material or cryogenic trapping [58]. CO_2 can then be recycled back to the process.

3.2. $LiPF_6$ Decomposition

$LiPF_6$ is known to be thermally and chemically unstable and the decomposition pathway is dependent on its environment [39–43,79]. In a dry and inert environment, anhydrous $LiPF_6$ generally decomposes thermally to form solid LiF and gaseous PF_5 (Eq. 1). In a humid environment, PF_5 eventually hydrolyzes to form POF_3 and gaseous HF (Eq. 2). However, $LiPF_6$

may directly endothermically decompose to form solid LiF, and gaseous POF_3 and HF in the presence of trace amounts of moisture/water (Eq. 3).

$$LiPF_6 \rightarrow LiF(s) + PF_5(g) \quad (1)$$

$$PF_5(g) + H_2O(g) \rightarrow POF_3(g) + 2HF(g) \quad (2)$$

$$LiPF_6 + H_2O \rightarrow LiF(s) + POF_3(g) + 2HF(g) \quad (3)$$

The thermal stability of $LiPF_6$ is poor, and in the literature its onset decomposition temperature is still highly debated. Kock et al., [41] report an onset point for the decomposition of anhydrous $LiPF_6$ at 134.84°C, whereas 114.46ºC is the onset point of the hydrolysis reaction. However, the degradation products POF_3 and HF were already observed below 90ºC in the presence of the electrolyte solvents, EC, EMC, DMC, and moisture [38,39,42]. The water concentration-sensitive hydrolysis degradation step was already observed at 300ppm H_2O at 87ºC [39].

3.3. Formation of Inorganic Phosphates by Hydrolysis of POF_3

In contact with water, POF_3 forms inorganic phosphates following the hydrolysis steps (Eqs. 4-6) [10,80]:

$$POF_3 + H_2O \rightarrow HPO_2F_2 + HF \quad (4)$$

$$HPO_2F_2 + H_2O \rightarrow H_2PO_3F + HF \quad (5)$$

$$H_2PO_3F + H_2O \rightarrow H_3PO_4 + HF \quad (6)$$

4. Experimental

The experiments conducted in the research presented in this thesis are described in this chapter. Two potential processes to recover the electrolyte from a spent LiB pouch cell are compared in this work; low temperature thermal treatment and sub-and supercritical CO_2 extraction. The method section is divided into two parts; low temperature thermal treatment process and sub- and scCO_2 extraction process, according to the processes studied. The sample preparation for both processes was similar and is therefore described in the same section. Following the methods, the instrumentation and analytical techniques are described.

4.1. Materials

Spent LiB pouch cells (NMC/graphite) produced for an EV application were used in this study. Details about the LiB cell cannot be provided due to a non-disclosure agreement. N_2 with a purity of 99.9% was used in the experiments. HNO_3 (>65%), acetone (>95%), acetonitrile (>99.9%), EMC (>99%), and EC (>98%) were purchased from Merck Millipore and dry ice from Cryotech. Liquid CO_2 with a purity of ≥99.99% (H_2O≤5 ppm w/w) was purchased from Air Liquide.

4.2. Sample preparation

Discharged spent NMC/graphite LiB battery pouch cells were stored for 2 days at -18°C to minimize the evaporation of the volatile electrolyte solvents during the cell opening. The pouch cell was opened, and the electrode stack (several layers of anode, separator, and cathode) removed manually by slicing along the edges with a scalpel. Before each experimental run, a scalpel was used to cut rectangular pieces from the electrode stack. Between each subsequent experimental run, the electrode stack was stored inside a sealed plastic bag at -18°C. The dimensions and sample weight in both processes were 9x1cm (11.07±0.95g) for the low temperature thermal treatment process and 14.7x0.5cm (8.81±0.72g) for the sub-scCO_2 extraction process.

4.3. Characterization of the Electrolyte Composition

The electrolyte composition was characterized using Fourier-transform infrared spectroscopy (FTIR) analysis and thermogravimetric analysis (TGA). For the FTIR measurements the sample was prepared as described in the previous section and was placed inside a combustion boat. The combustion boat was then inserted in a quartz tube and a N_2 flow of 340 ml/min was applied. The quartz tube exhaust was passed through a gas collection chamber placed inside the FTIR instrument. The exhaust at room temperature was then monitored every minute.

The TGA measurement was conducted after placing one layer of the electrode stack (20.99±0.01 mg), including cathode, separator and anode, inside an Alumina boat.

4.4. Low Temperature Thermal Treatment Process

4.4.1. Set-up

A schematic of the experimental set-up of the low temperature thermal treatment process is presented in Figure 2. A quartz tube was placed inside a tube furnace. The outlet of the quartz tube was either connected to a collection vial placed in a cold trap with a mixture of dry ice and acetone at -78°C (Route A) or in a gas cell with flat glass CaF_2 windows and an optical path length of 10 cm (Route B). In both cases, a gas washing bottle filled with 50 ml MQ water was subsequently connected before the release of the exhaust to the environment. N_2 flow was controlled by a metering valve and measured by a flowmeter. The tube furnace temperature was set to 90°C, 110°C, 130°C, and 150°C, and was monitored by a thermocouple connected to a data logger (TC-08, Pico Technology).

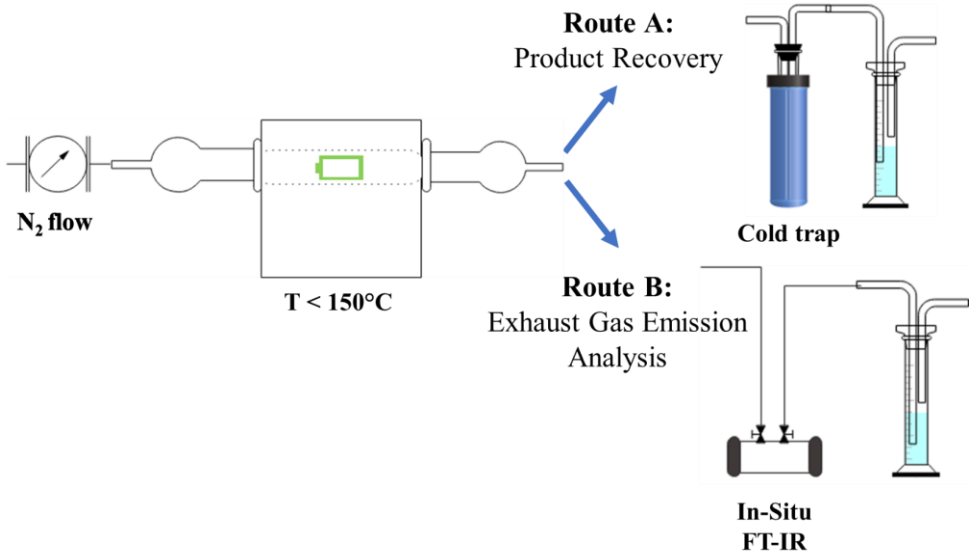

Figure 2. Illustration of the experimental set-up of the low temperature thermal treatment process.

4.4.2. Methods

A flow-sheet of the experimental method of the low temperature thermal treatment process is shown in Figure 3.

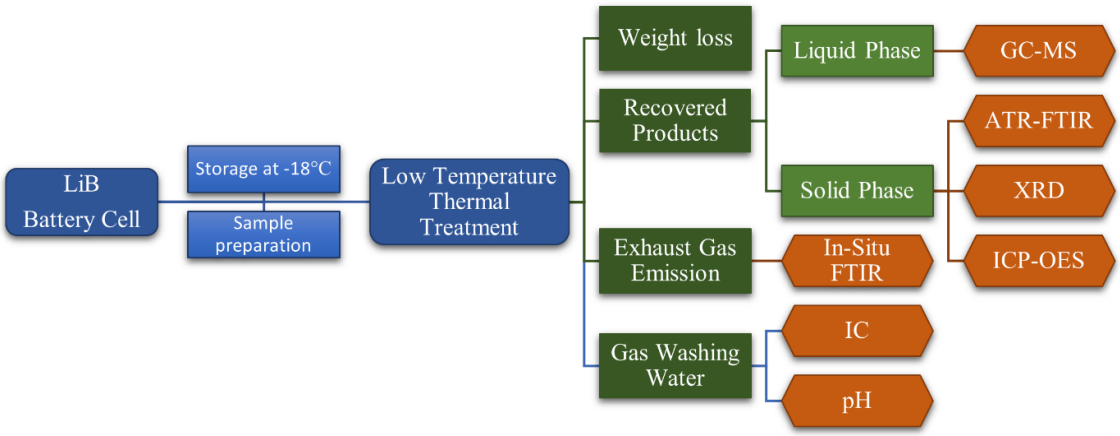

Figure 3. Flow-sheet of the experimental method of the low temperature thermal treatment process

The LiB sample was placed inside a ceramic combustion boat. To equilibrate the N_2 environment inside the quartz tube, the combustion boat was first inserted into the quartz tube outside the tube furnace. After 5 minutes of equilibration, the ceramic combustion boat was pushed into the center of the tube furnace under N_2 atmosphere. After a low temperature thermal treatment process time of 3 hours, the combustion boat was removed from the tube furnace at the reaction temperature and subsequently cooled at room temperature. Before and after the low temperature thermal treatment process, the battery sample weight was measured with a high-precision scale under air.

The low temperature thermal treatment process for each temperature setting (90ºC, 110ºC, 130ºC and 150ºC) was conducted in triplicate in random order. In route A, the exhaust gas was directly cryogenically trapped in a sample vial placed in a cold trap with a mixture of dry ice and acetone at -78°C. The recovered liquid phase product was characterized by gas chromatography coupled with mass spectroscopy (GC-MS) after dilution in acetonitrile (1:150). The solid phase product was collected from the walls of the quartz tube outside the tube furnace after the setup cooled. The sample was characterized by attenuated total reflection (ATR)-FTIR by placing the solid phase product on top of the diamond of the universal ATR accessory and applying a sufficient force with the pressure arm. Subsequently, the solid phase sample was ground using a mortar for X-ray diffraction (XRD) analysis, and inductively coupled plasma optical emission spectroscopy (ICP-OES) analysis. For ICP-OES analysis the samples were further dissolved in 0.5 M HNO_3 and subsequently filtered.

In route B, the exhaust gas of the thermal treatment processes was frequently monitored over the entire process time of 3 hours by FTIR spectroscopy in the range of 4000cm^{-1} - 900cm^{-1}. Therefore, the exhaust gas was passed through a gas collection chamber situated inside the FTIR instrument before bubbling through the gas washing bottle.

In all the experimental runs the exhaust gas was washed using a gas washing bottle filled with 50 ml MQ water before its release into the environment. The gas washing water was analyzed with ion chromatography (IC) and the pH was measured. For the IC analysis, the samples were further diluted (1:30) in MQ water.

4.5. Sub-and Supercritical CO_2 Extraction Process

4.5.1. Set-up

The supercritical fluid technology system used in this work is illustrated in

Figure *4*. The system was constructed inside a fume hood. Liquid CO_2 provided by a pressure cylinder was pressurized by a syringe pump system (ISCO 260D, Teledyne ISCO) and heated by an external heat system (Model F10 & CM, Julabo). Manual valves were used to direct the gas flow into the stainless-steel reactor (50 ml) to pressurize the reactor with CO_2. The reactor was thermostated by water pipes connected to an external thermostat (Model F12 & ED, Julabo). A thermometer and manometer were used to monitor the pressure and temperature in the reactor volume. The flow-rate was controlled by a meter valve and monitored using a flow-meter. To avoid freezing the CO_2, the exhaust meter valve temperature was controlled to 40±5°C by a thermostat. The exhaust was cryogenically trapped in a sample vial placed in a cold trap with a mixture of dry ice and acetone at -78°C. A gas chamber was connected to the cold trap outlet for in-situ FTIR analysis of the exhaust emission. After bubbling through a gas washing bottle filled with 50 ml MQ water the exhaust gas was released to the environment.

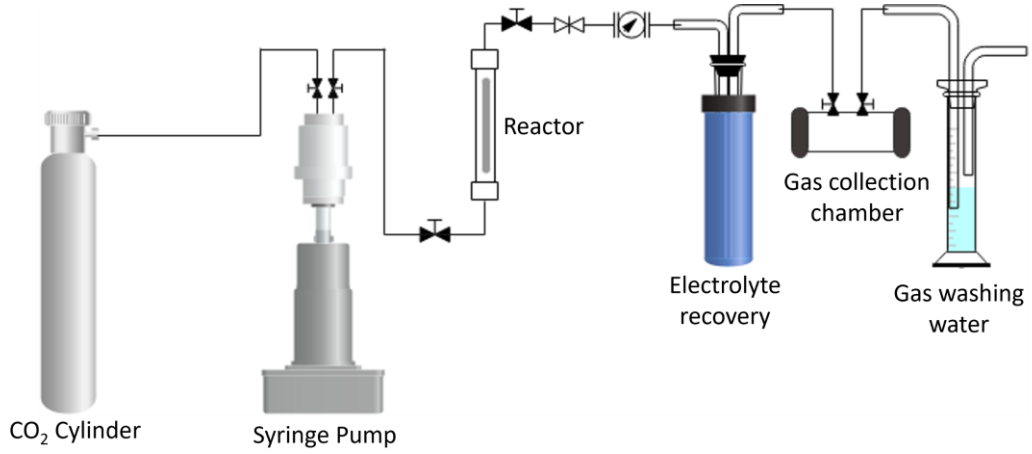

Figure 4. Illustration of the scCO₂ extraction process set-up.

4.5.2. Methods

The LiB electrode stack sample was placed inside the reactor and the reactor was subsequently leak-tight closed using wrenches. Temperature-controlled water pipes were then extensively whirled along the reactor to control the process temperature (15°C - 55°C with uncertainties of 2ºC). The reactor was pressurised to the experimental pressure (60 - 120 bar with uncertainties of 4 bar) with the syringe pump system. Two different extraction modes, static and dynamic extraction, were applied. In the static extraction mode, the reactor was filled with CO_2 by the syringe pump system to constant pressure and temperature and after the extraction time this was released out of the reactor. In the dynamic extraction mode, a constant CO_2 flow was applied over the entire extraction time while maintaining a constant process pressure and temperature. A static equilibration time of 3 min was used to stabilize the system at the process temperature and pressure conditions. Then a constant CO_2 flow (8.5±1 ml/min) was applied for 30 minutes. After the constant CO_2 flow-through experimental time of 30 min, the reactor was entirely depressurised, the water pipes were removed, the reactor was opened using wrenches and the electrode stack sample removed from the reactor. The mass of the electrode stack

sample was determined before and after the experimental run by a precision scale. All experiments were conducted in triplicate.

The exhaust was passed through a collection vial inside the cold trap to collect the extracted product. Subsequently, the recovered liquid phase product was analysed by ATR-FTIR, GC-MS and ICP-OES. For the ATR-FTIR analysis 200 µl of each collected sample was placed on top of the diamond surface of the universal ATR accessory. GC-MS analysis was performed after the sample was diluted (1:150) in acetonitrile. For ICP-OES analysis 50 µl of the recovered liquid sample was dissolved in 0.5 M HNO_3 (4.5ml) and subsequently filtered.

The cold trap outlet exhaust was frequently monitored over the entire process time of 30 minutes using FTIR spectroscopy in the range of 4000cm^{-1}-900cm^{-1}. Therefore, the exhaust gas was passed through a gas collection chamber situated inside the FTIR instrument before bubbling through the gas washing bottle.

The active cathode material was scratched from the cathode material using a razor blade for XRD analysis and was collected in a sample vial. After adding acetone, the active cathode material powder was distributed by sonication. The sample was then distributed on the surface of a silicon crystal sample holder by dropping a few droplets in its center. The sample was dried by evaporating the acetone and the process was repeated until an evenly distributed surface was achieved on the crystal sample holder.

4.6. Instrumentation and Analytical Methods

4.6.1. Furnace

A horizontal electrical tube furnace (RT 50-250/13, Nabertherm) and a controller (P330, Nabertherm) with a maximum operating temperature of 1300ºC was used for the recovery of the electrolyte by low temperature thermal treatment. The quartz tube inner diameter was 30 mm. Ceramic combustion boats (120 x 20 x 13 mm) were obtained from VWR.

4.6.2. Weight loss determination after the electrolyte separation process

The weight loss of the electrode stack sample was associated with the amount of the separated electrolyte in the corresponding processes. The sample weight loss was determined in weight percentage (wt%) and was calculated according to Eq. (7):

$$Weight\ loss = \left(1 - \frac{m_{after}}{m_{initial}}\right) \times 100 \qquad (7)$$

where $m_{initial}$ is the initial sample weight and m_{afrer} is the sample weight after the electrolyte separation process.

4.6.3. Thermogravimetric Analysis (TGA)

Thermogravimetric analysis (TGA) was carried out using a thermogravimetric analyzer (Q500, TA Instruments) in a temperature range between 20°C and 300°C and a constant N_2 gas flow of 100 ml/min. A specific analysis method of the equipment was used to obtain high-resolution results. Based on the sample weight change, the heating rate of the furnace was automatically reduced and controlled by the equipment. The heating rate was a maximum of 5°C/min with a high-resolution sensitivity of 4.0 and a resolution of 5.0. The TGA sample weight was 20.99±0.01 mg.

4.6.4. Fourier-Transform Infrared Spectroscopy (FTIR)

Fourier-transform infrared spectroscopy (FTIR) was used to analyze the exhaust gas in both processes. The FTIR spectra were continuously recorded by a FTIR spectrometer (Spectrum Two, Perkin Elmer) in the range of 4000cm^{-1} - 900cm^{-1} with a resolution of 4cm^{-1} over the entire process time. The scan time per spectrum was selected to be 40 seconds, which corresponded to approximately 12 scans. Reference gas phase spectra of EC and EMC were obtained by evaporation of a few droplets of liquid phase EMC and EC, separately, inside the gas cell while monitoring the FTIR spectra. The exhaust composition evolution of the strong characteristic peaks of the detected components were plotted over the entire experimental time.

The universal attenuated total reflection (ATR) accessory of the FTIR spectrometer (Spectrum Two, Perkin Elmer) was used to characterize the recovered solid phase product after the thermal treatment process and the recovered liquid phase product after the sub-scCO_2 extraction process. The ATR FTIR spectra were recorded in a range of 4000 cm^{-1} to 450 cm^{-1} with a resolution of 2 cm^{-1} and a total of 32 scans.

4.6.5. Gas Chromatography – Mass Spectroscopy (GC-MS)

Gas chromatography coupled with mass-spectroscopy (GC-MS, 7890A, Agilent Technologies) with an Agilent HP-5MS 5% Phenyl Methyl Silox column (30 m x 250 μm x 0.25 μm) was used to analyze the recovered liquid product. The samples were diluted with acetonitrile

(1:150) and then injected at 250°C with a split ratio of 1:100 and a purge flow of 3 ml/min. Helium as carrier gas with a column flow of 1 mL/min was selected. The selected oven program for the liquid products recovered by low temperature thermal treatment and sub-supercritical fluid extraction are shown in Table 2. The mass spectrum was obtained in the electron ionization (EI) mode at 230°C ion source temperature and 70eV filament voltage in a range of 15-300 m/z**.**

Table 2. Parameters of the oven program for the GC-MS analysis of the recovered liquid product.

	Low Temperature Thermal Treatment	**Sub-Supercritical CO_2 Extraction**
Initial temperature	40ºC, 1 min	40ºC, 1 min
Heating rate	30ºC/min	20ºC/min
Final temperature	230ºC, 3 min	230ºC, 2 min

4.6.6. Inductively Coupled Plasma - Optical Emission Spectrometry (ICP-OES)

Inductively coupled plasma - optical emission spectrometry (ICP-OES, ThermoFisher Scientific, iCAP PRO) was used for elemental analysis of the recovered liquid and solid products. The recovered solid product in the low temperature thermal treatment process was dissolved in 0.5 M HNO_3 (5 ml) and subsequently filtered. The recovered liquid product (50 µl) in the sub-sc-CO_2 process was dissolved in 0.5 M HNO_3 (4.5 ml) and filtered. Li, Zn, Ni, Co, Fe, Mn, Cu, Al and P prepared by dilution in 0.5M HNO_3 were used as standards for the elemental analysis.

4.6.7. X-Ray Diffraction Analysis (XRD)

A Bruker D8 Advance was used to determine the crystallographic structure of the collected solid phase product in the low temperature thermal treatment process. The diffraction pattern in the 2Θ range of 10 -55º was obtained using a Cu radiation source with a Kα wavelength of 1.5406 Å. The operating voltage and current were 40 kV and 40 mA, respectively. Before the XRD analysis, the collected solid phase product was pulverized with a mortar.

A Bruker D8 Discover (EIGER2R 500K detector) was used analyze the structural changes of the active cathode material before and after the sub-scCO_2 electrolyte extraction process in a 2Θ range of 10º - 80º. A Cu radiation source with a characteristic Kα wavelength of 1.5406 Å was used and the operating voltage and current were set to 40 kV and 40 mA, respectively.

4.6.8. Ion Chromatography (IC)

Ion chromatography (IC, Metrohm 771 IC Compact, DX-100, Dionex) was used to analyze the gas washing water after the low temperature thermal treatment process. The samples were diluted with MQ water (1:30) and then injected (20 µl) into the column (DionexIonPac AG4A- SC, 4 x 50 mm, ThermoFisher Scientific) for anion analysis. As the eluent, a carbonate buffer (1.7 mM $NaHCO_3$, 1.8 mM Na_2CO_3) was used and MQ water was used as a background. The presence of F^- and PO_4^{3-} was confirmed via the retention time of standard solutions.

5. Results

The results chapter is divided into three sections. The first section describes the findings of the characterization of the electrolyte composition in the spent LiB sample. The following sections describe the results of the two different studied processes; low temperature thermal treatment and sub-and supercritical CO_2 extraction.

5.1. Characterization of the Electrolyte Composition

The exhaust composition of the LiB electrode stack sample at room temperature (24±2ºC) was analyzed by In-Situ FT-IR spectra using a constant N_2 flow of 340 ml/min. Figure 5 shows the FT-IR spectra of the exhaust after 1, 3, and 5 minutes. The gas phase spectra of pure DMC, EMC, and EC are plotted as a reference. The vibrational peaks at 1780 cm^{-1} (νC=O), 1463 cm^{-1} (CH_3 sym. def.), and 1295 cm^{-1} (ν_aO-C-O) originate from DMC [81], whereas the peaks at 1772 cm^{-1} (νC=O), 1378 cm^{-1} (CH_3) and 1370 cm^{-1} were assigned to EMC [82]. The peaks at 1876 cm^{-1}, 1868 cm^{-1}, and 1860 cm^{-1} of the exhaust gas correspond to the characteristic peaks of EC in gas phase [83]. Hence, vibrational peaks corresponding to DMC, EMC, and EC were observed in the LiB sample exhaust at room temperature.

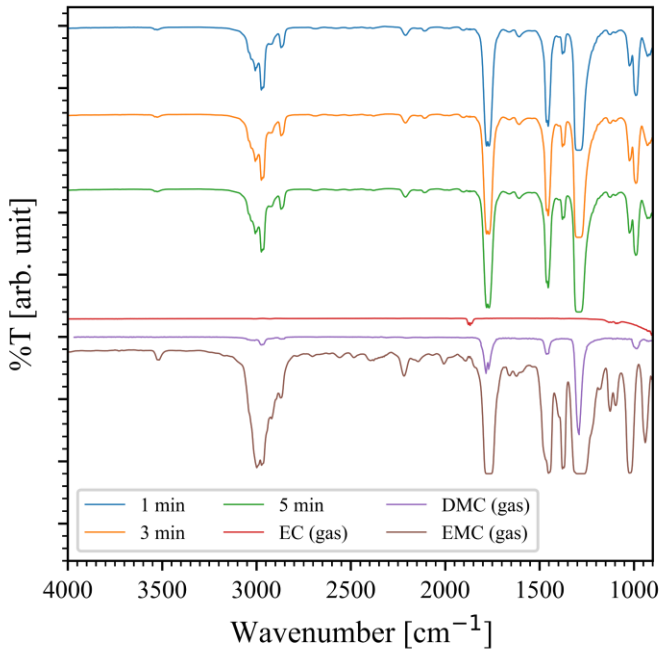

Figure 5. FT-IR spectra of the LiB sample exhaust gas at room temperature (24ºC) after 1, 3, and 5 min. The gas phase spectra of DMC, EMC, and EC are plotted as a reference.

Thermogravimetric analysis (TGA) of the spent LiB electrode stack was conducted to verify the electrolyte solvent mixture composition based on their boiling points. Additionally, the TGA result was used to set the furnace temperature conditions for the low temperature thermal treatment process. Figure 6 presents the thermogravimetric (TG) and the differentiate thermogravimetric (DTG) curve of the electrode stack sample (20.99±0.1mg) in the temperature range between 20°C and 300°C. The determined weight loss of the electrode stack was 9.34wt%. In the DTG curve, three peaks at 96°C, 109.6°C, and 128.9°C were clearly observed. The temperatures are in alignment with the boiling points of DMC (90°C), and EMC

(107°C). The peak at 128.9°C was associated with the onset decomposition temperature of $LiPF_6$, which was reported to be 134.84°C [21]. A peak corresponding to the boiling point temperature of EC at 248°C was not observed since EC most likely evaporated along with the other substances before its boiling point was reached. Hence, the electrolyte solvent mixture was believed to be composed of DMC, EMC and, EC, as FTIR and TGA results evince.

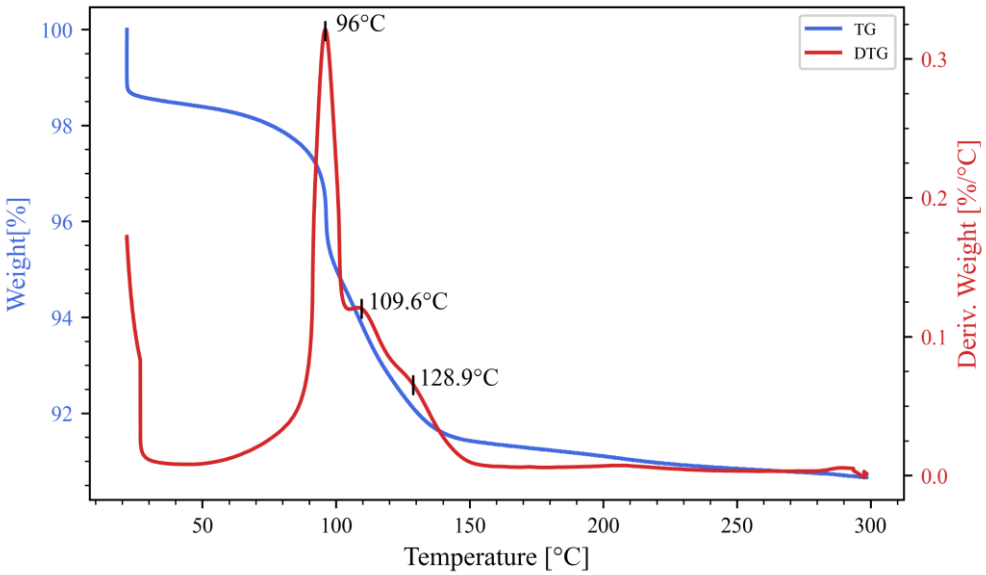

Figure 6: Thermogravimetric (TG, blue) and differentiate thermogravimetric (DTG, red) curves of the LiB electrode stack sample.

The DTG curve remained steady after 150°C and further peaks between 150°C and 300°C were not observed. Accordingly, the maximum thermal treatment process temperature was set to 150°C. The other furnace temperatures were set to 90°C, 110°C, and 130°C based on the DTG curve peaks at 96ºC, 109.6ºC, and 128.9ºC.

5.2. Low Temperature Thermal Treatment Process

The sample weight loss in weight percent (wt%) at the different process temperatures 90ºC, 110ºC, 130ºC, and 150ºC is plotted in Figure 7. The weight loss converged at a process temperature of 130ºC to 13.9±0.1wt%. It is noticeable that with increase in temperature, the standard deviation of the triplicates decreased.

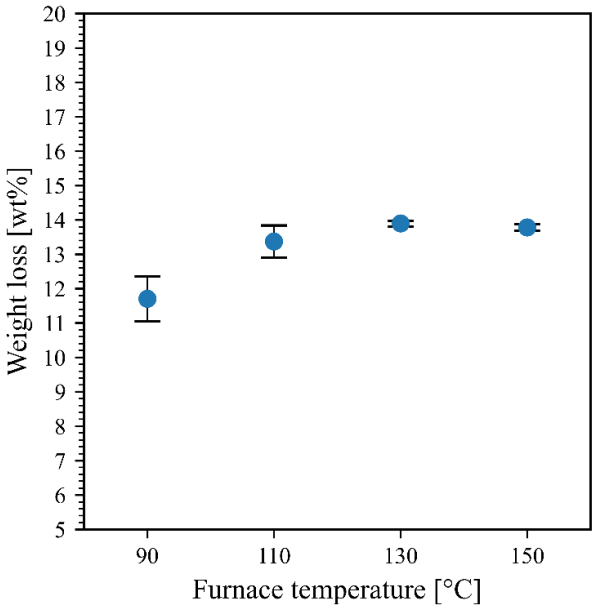

Figure 7. LiB sample weight loss given in weight percentage (wt%) after the low temperature thermal treatment for 3 hours under constant N_2 flow at various temperature conditions.

After the electrolyte separation by the low temperature thermal treatment, both a liquid and solid phase product were collected. The composition of the liquid phase product was analyzed with GC-MS and the obtained chromatographs are plotted in Figure 8. The peaks with retention times at 2.33 min, 2.81 min, and 4.59 min were clearly identified as DMC, EMC, and EC, according to the NIST 08 library.

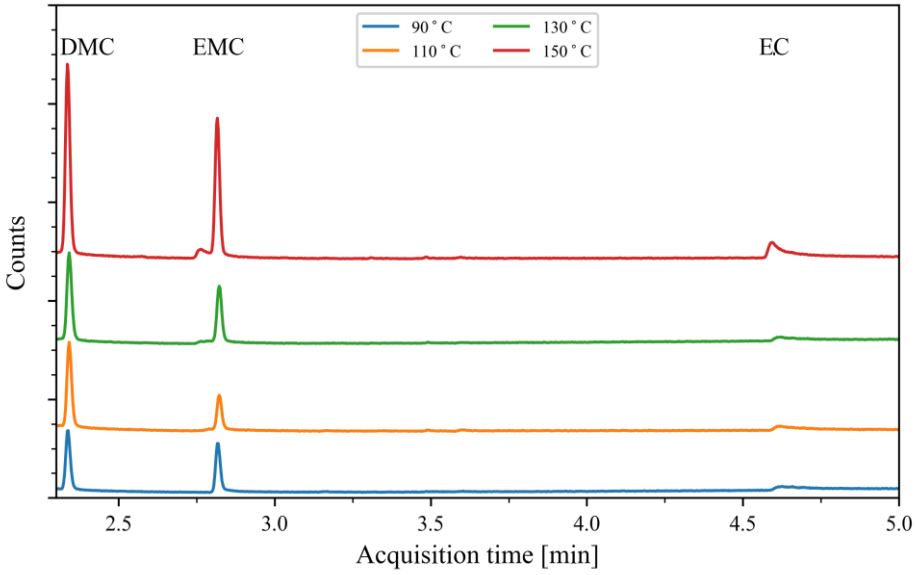

Figure 8. Chromatograms (GC-MS) of the recovered electrolyte at different thermal treatment process temperatures of 90°C, 110°C, 130°C, 150°C.

Roughly 0.3g (≈ 20-25% of weight loss) of the crystalline condensate residue was collected from the quartz tube walls after the processes, as shown in Figure 9. To determine its composition, the recovered solid phase product was analyzed by ATR-FTIR, XRD, and ICP - OES.

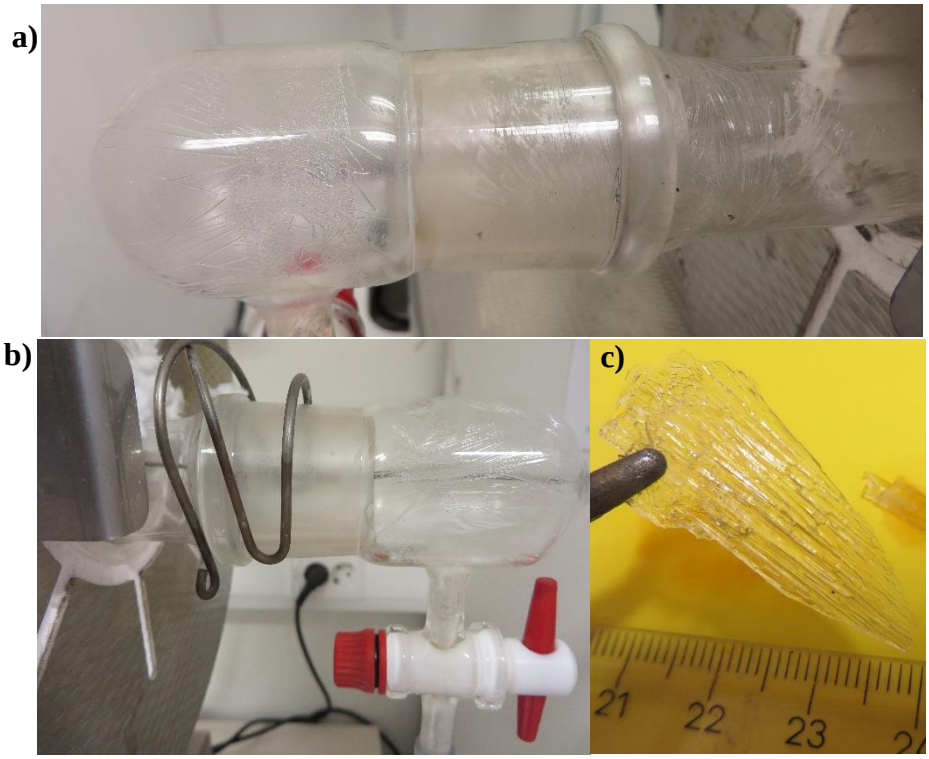

Figure 9. a) and b) Quartz tube wall coated with the condensed solid phase product after the low temperature thermal treatment. c) Zoomed in image of the collected solid phase product.

The ATR-FTIR spectra of the recovered crystalline solid phase residue collected after the low temperature thermal treatment process at 110ºC, 130ºC, and 150ºC are plotted in Figure 10 together with the solid phase EC spectrum used as a reference. The ATR-FTIR spectra of the recovered crystalline product clearly matches the EC reference. Minor peaks between 1050 cm^{-1} and 450 cm^{-1} matching with the vibrational modes of POF_3 (a,c) and $LiPF_6$ (b,d) were also observed in the solid phase product spectra.

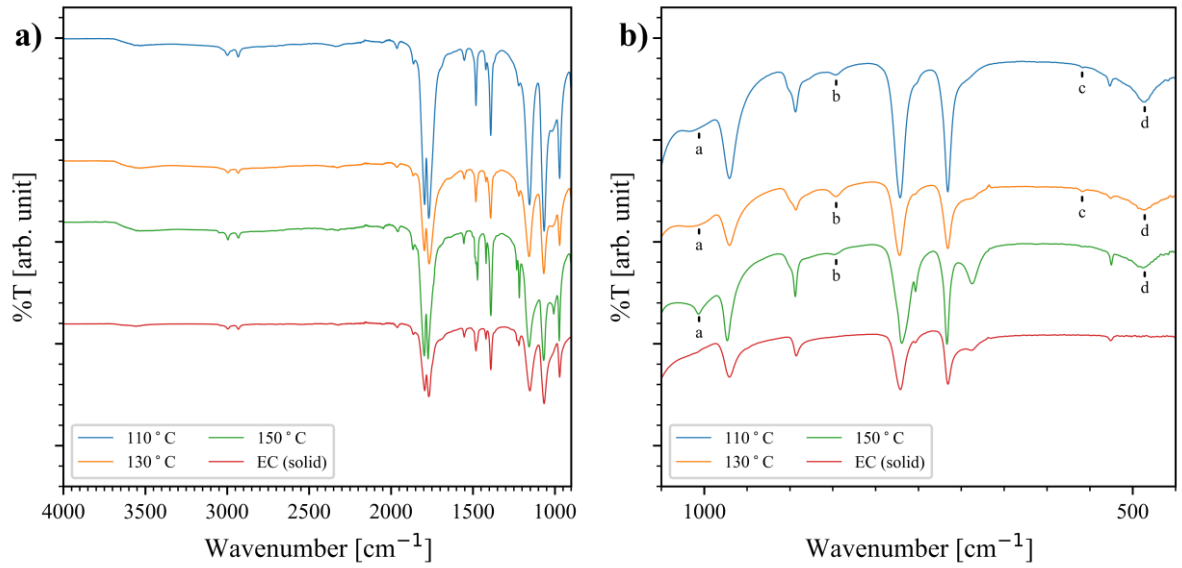

Figure 10. ATR-FTIR spectra between a) 4000-900 cm^{-1} and b) 1050-450 cm^{-1} of the quartz tube residue collected after the low temperature thermal treatment experimental runs at 110°C, 130°C, and 150°C. EC in solid phase is given as a reference.

The diffraction pattern of the XRD analysis of the recovered solid phase product in the 2Θ range from 10º to 55º is plotted in Figure 11. The diffraction peaks were clearly assigned to EC with monoclinic crystal structure (PDF Card No: 00-008-0768).

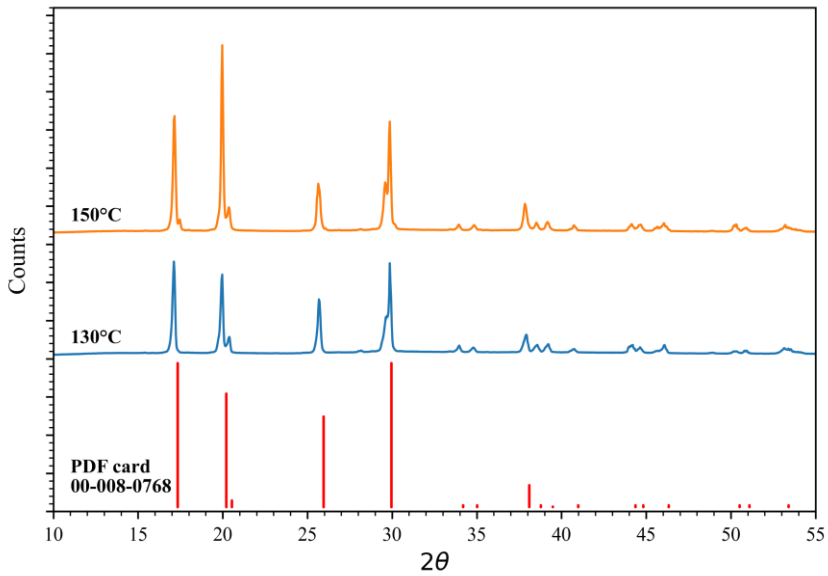

Figure 11. XRD pattern in the range from 10° to 55° 2Θ of the collected solid phase product after the thermal treatment process at 130°C and 150°C.

ICP-OES analysis showed elemental impurities of Li (0.8 ppm), Mn (2.3 ppm), Co (0.94 ppm), Cu (1.29 ppm), Ni (0.57 ppm), and Al (0.16 ppm).

The process exhaust gas over the entire experimental period was analysed with in-situ FTIR. Figure 12 shows the recorded FT-IR spectra after 1, 15, 30, 60, 90, 120, and 180 min at the different process temperatures (90ºC, 110ºC, 130ºC, and 150ºC). At all temperature conditions, characteristic peaks assigned to the electrolyte solvents DMC, EMC and EC were detected. After 15 minutes at all temperature conditions, characteristic peaks assigned to HF (4000 cm^{-1}

to 3600 cm^{-1}) and POF_3 (1428 cm^{-1}, 1416 cm^{-1}, 1404 cm^{-1}, and 991 cm^{-1}) were additionally detected [38–40].

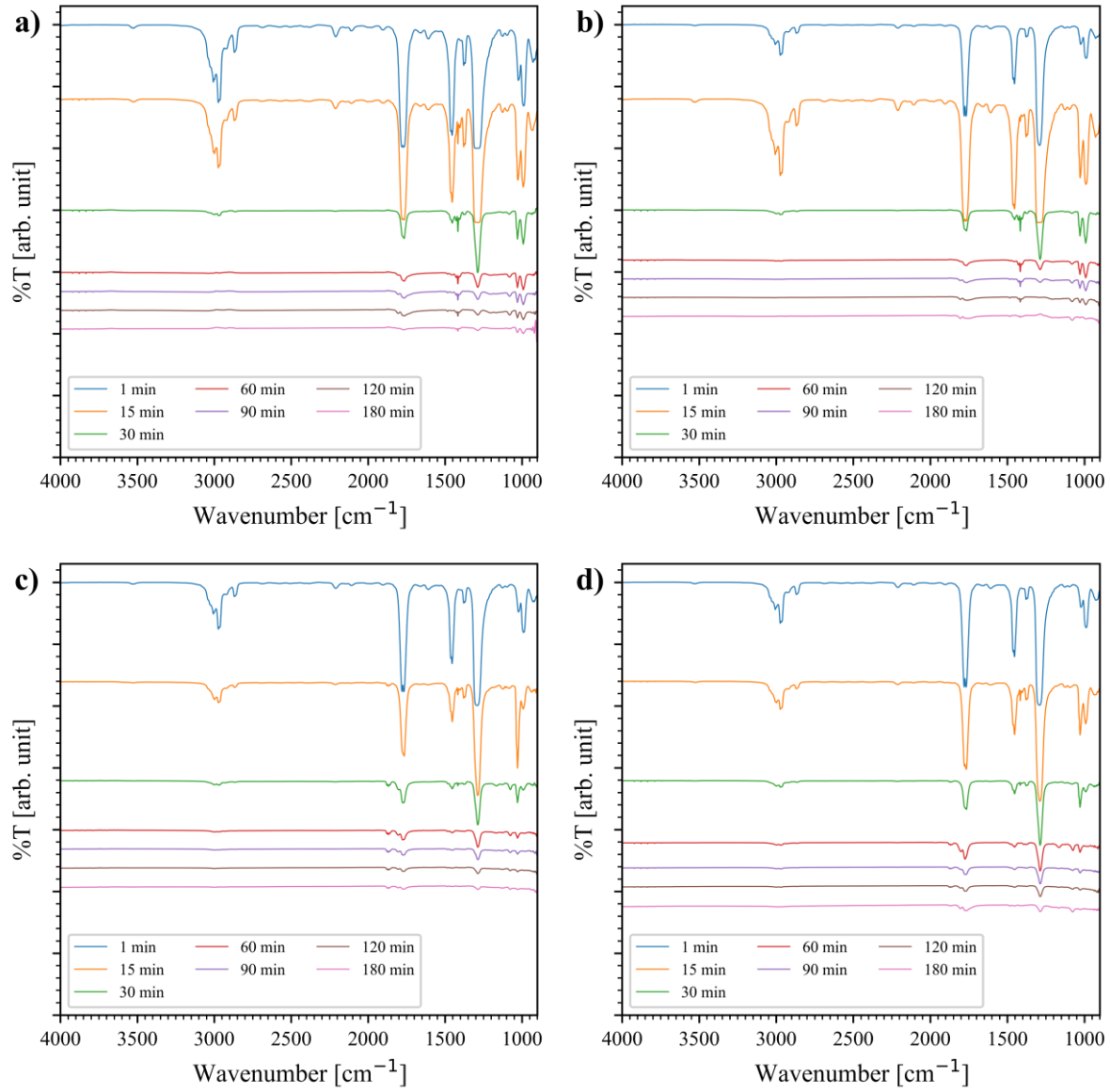

Figure 12. In-Situ FT-IR spectra of the process exhaust gas after 1, 15, 30, 60, 90, 120, and 180 min at a) 90°C, b) 110°C, c) 130°C, and d) 150°C.

The electrolyte solvent separation rate was determined based on the vanish point of the relative absorption intensity of the electrolyte solvents DMC and EMC. Owing to the strong peak intensity and selectivity, the relative absorption intensity of the vibrational peaks at 1780 cm^{-1} belonging to νC=O of DMC and at 1284 cm^{-1} corresponding to νO-C-O vibration of EMC over the entire process time is plotted in Figure 13. It is noteworthy that the equilibration time, the time before feeding the sample to the hot zone of the furnace, is denoted as -5 to 0 min.

Before the combustion boat was exposed to the process temperature - the equilibration time denoted as -5 to 0 min - relative absorption intensities above 74% (C=O peak, DMC) and 90% (O-C-O peak, EMC) were already observed in the FT-IR spectra for all temperature conditions. When exposed to the process temperatures, an immediate raise to 100% was observed. Eventually, the relative absorption intensity started to vanish after 40 minutes, before finally levelling off at around 60 minutes for DMC and 80 minutes for the EMC peak.

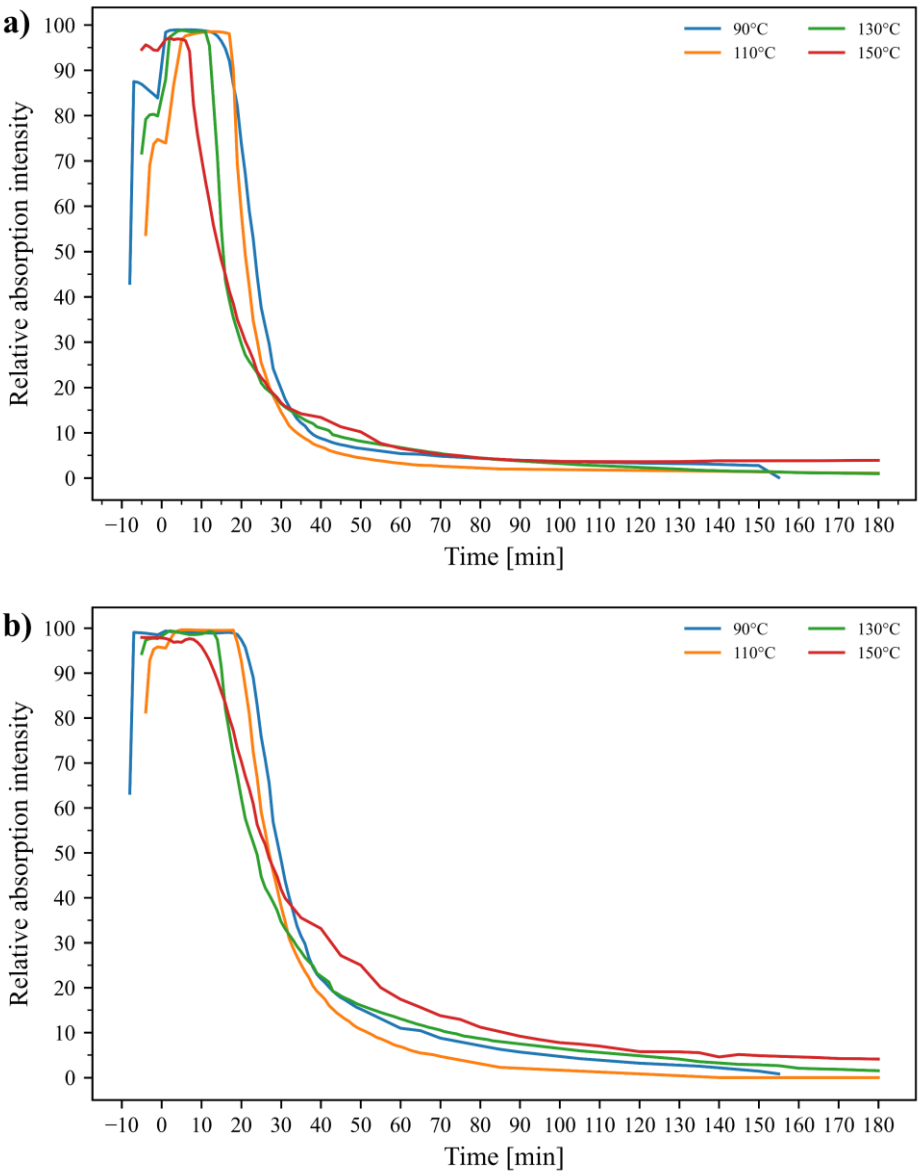

Figure 13. Relative absorption intensity over the thermal treatment process time of 180 minutes of the a) C=O peak of DMC at 1780 cm^{-1} and b) O-C-O peak of EMC at 1284 cm^{-1}.

The time-dependent relative absorption intensity changes of the strong characteristic peaks of HF (3878 cm^{-1}) and POF_3 (1416 cm^{-1}) were plotted over the entire process period of 180 minutes, as shown in Figure 14. The vibrational peaks of HF and POF_3 appeared simultaneously between 4 and 10 minutes, depending on the process temperature. Furthermore, it can be observed that a higher process temperature causes a shorter $LiPF_6$ hydrolysis degradation time span. At process temperatures of 130ºC and 150ºC the relative absorption intensity diverged to a constant level after a maximum of 70 minutes. Below 130ºC, by contrast, the POF_3 peak decreased but did not level off during the entire process time of 180 minutes.

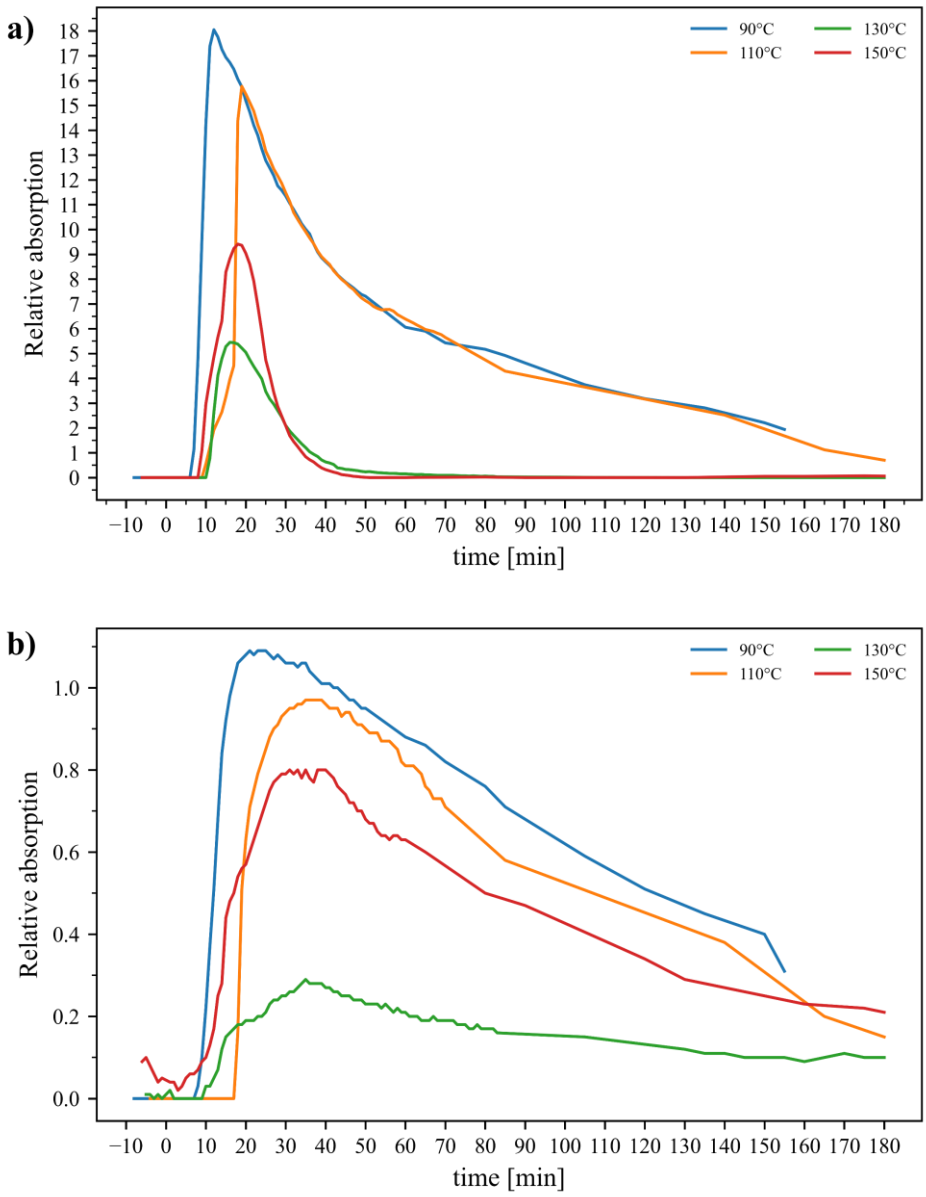

Figure 14. Relative absorption intensity over the entire process time of the characteristic peaks of a) POF_3 at 1416 cm^{-1}, and b) HF at 3878 cm^{-1}.

The results of the IC analysis of the gas washing water are plotted in Figure 15. The distinctive peaks at retention times at 2.8 and 10.8 minutes were assigned to F^- and PO_4^{3-} based on the retention time of standard solutions.

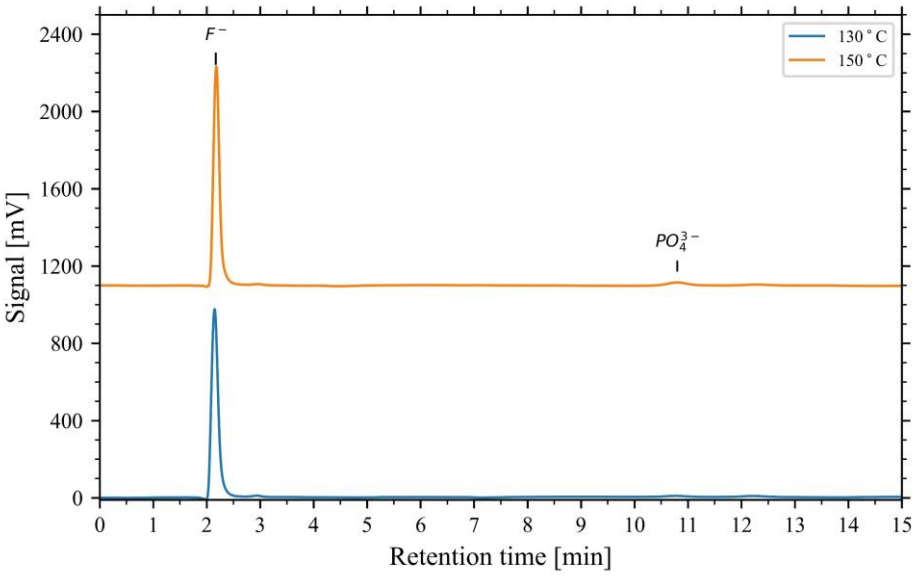

Figure 15. IC chromatograph of the gas washing water of the thermal treatment process at process temperature of 130°C and 150°C.

5.3. Sub- and Supercritical CO_2 Extraction Process

The influences of pressure (60-120 bar), temperature (15-55°C) and the corresponding estimated CO_2 density on the sample weight loss in weight percentage (wt%) and the electrolyte separation efficiency from the electrode sample are plotted in Figure 16. The electrolyte separation efficiency was calculated based on the highest electrolyte separation efficiency achieved by the low temperature thermal treatment process, which was 13.9±0.1wt% at 130ºC. The total electrolyte weight was then adjusted to 14.2wt% of the electrode stack sample with consideration of the LiF residues in the sample after the $LiPF_6$ decomposition. A value of 88.2% of the total electrolyte amount was attributed to the electrolyte solvent, which corresponds to 12.5wt% of the electrode stack. The $LiPF_6$ contribution was estimated to be 11.8%, which corresponded to 1.7wt% of the electrode stack.

The influence of the pressure conditions at 29ºC is plotted in Figure 16a. A maximum electrolyte separation efficiency of 66.1% (9.39±0.17wt%) was achieved at 80 bar. The electrolyte separation efficiency did not increase further with pressure, but instead rather slightly decreased to 63.5% (9.02±0.07wt%) at 120 bar. The influence of the temperature conditions at 80 bar is plotted in Figure 16b. An increase in process temperature above 29°C resulted in a (linear) decrease in separation efficiency from the LiB electrode stack. At 29°C and below, the electrolyte separation efficiency remained rather constant at 66.1% (9.39±0.17wt%) within the standard deviation of the triplicates. The process pressure and temperature conditions in the extraction process have a direct impact on the CO_2 density. The CO_2 density at the different process conditions was estimated and plotted against the weight loss (wt%) and separation efficiency (%), as shown in Figure 16c. A clear dependence of the electrolyte separation efficiency on the CO_2 density can be observed. The electrolyte separation efficiency was almost constant with respect to the standard deviation of the triplicate in the CO_2 density range of 600 kg/m^3- 900 kg/m^3. Below a CO_2 density of 600 kg/m^3, a decrease of the electrolyte separation efficiency was observed. The maximum electrolyte separation efficiency of 66% was reached at a CO_2 density of 715 kg/m^3.

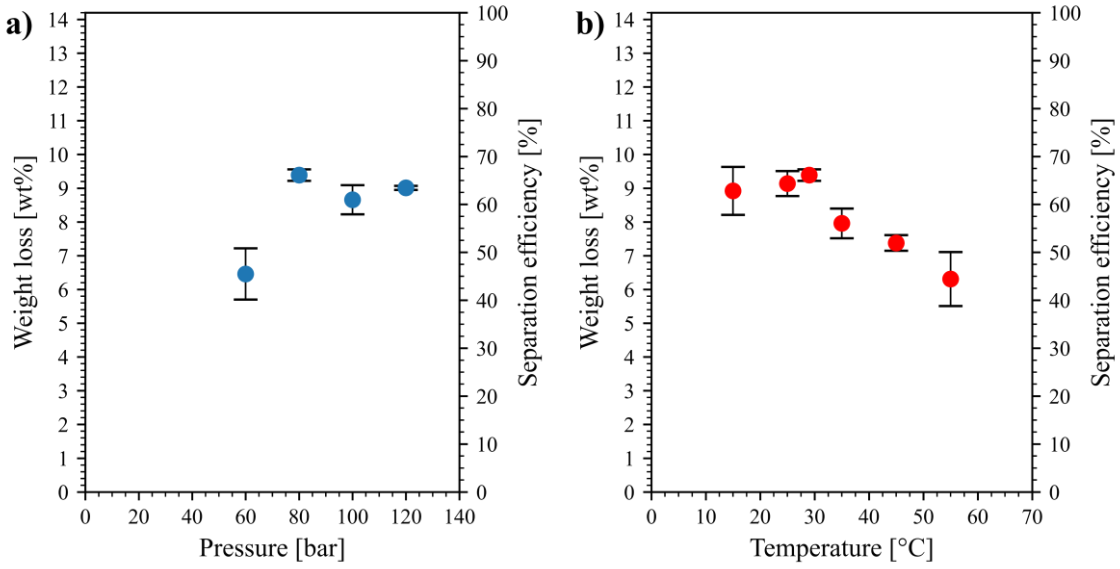

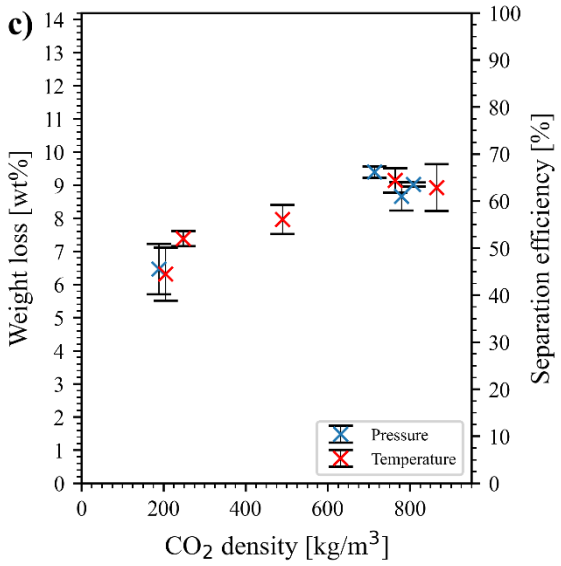

Figure 16. LiB sample weight loss in weight percentage (wt%) and corresponding electrolyte separation efficiency after the sub-and scCO₂ extraction process with different process parameters. a) dependence of pressure at 29°C, b) dependence of temperature at 80 bar, c) dependence of CO₂ density.

The composition and purity of the collected extracts were analyzed with GC-MS and ICP-OES. The GC-MS chromatographs of the collected extract at the different CO_2 process densities plotted in Figure 17a show peaks at acquisition times of 2.35, 2.93, and 5.31 minutes. In addition, minor peaks at 3.18, 3.35, 3.63, and 3.85 minutes were detected in the focused plot in Figure 17b. The peaks at 2.35, 2.93, and 5.31 minutes were assigned to the organic electrolyte solvents DMC, EMC and EC, whereas the peaks at 3.18, 3.63, and 3.85 minutes were assigned to the electrolyte decomposition products dimethyl fluorophosphate (DMFP), diethyl carbonate (DEC), and ethyl methyl fluorophosphate (EMFP). The peak at 3.35 minutes was assigned to the electrolyte additive vinylene carbonate (VC).

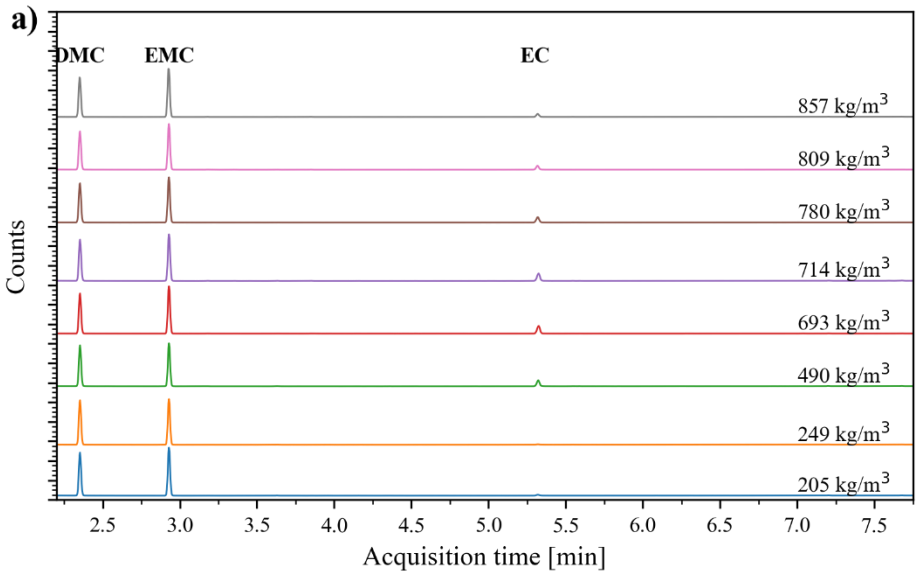

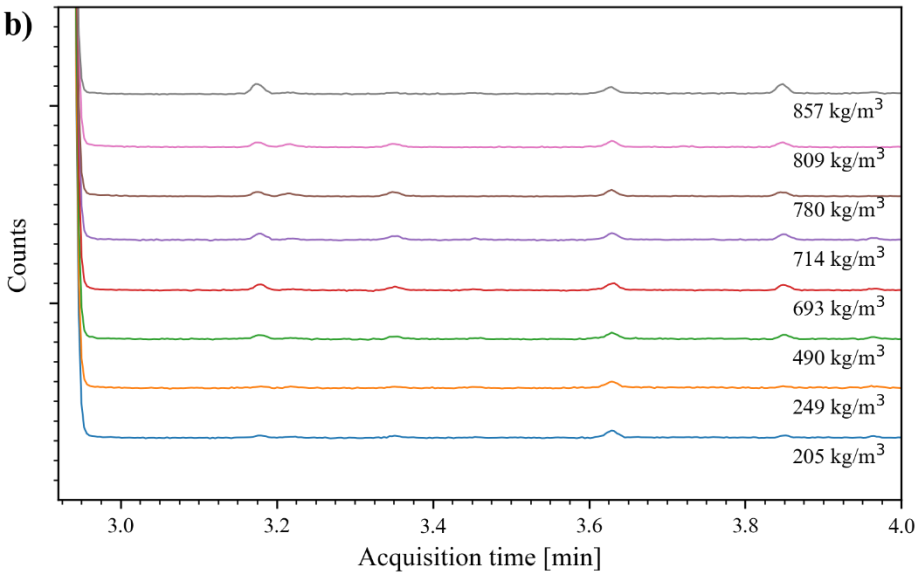

Figure 17. a) GC-MS chromatogram of the collected liquid phase product at various CO_2 densities and (b) focused between 2.9 and 4 minutes.

The quantitative analysis of the collected extract in respect to the CO_2 process density is plotted in Figure 18. The proportion of EC was observed to be dependent on the CO_2 process density. Less than 2% of EC was detected at densities below 300 kg/m^3, whereas the share of EC in the collected extract increased to 9.7% with the increase of CO_2 density to 714 kg/m^3 and then decreased to 3.9% at 857 kg/m^3.

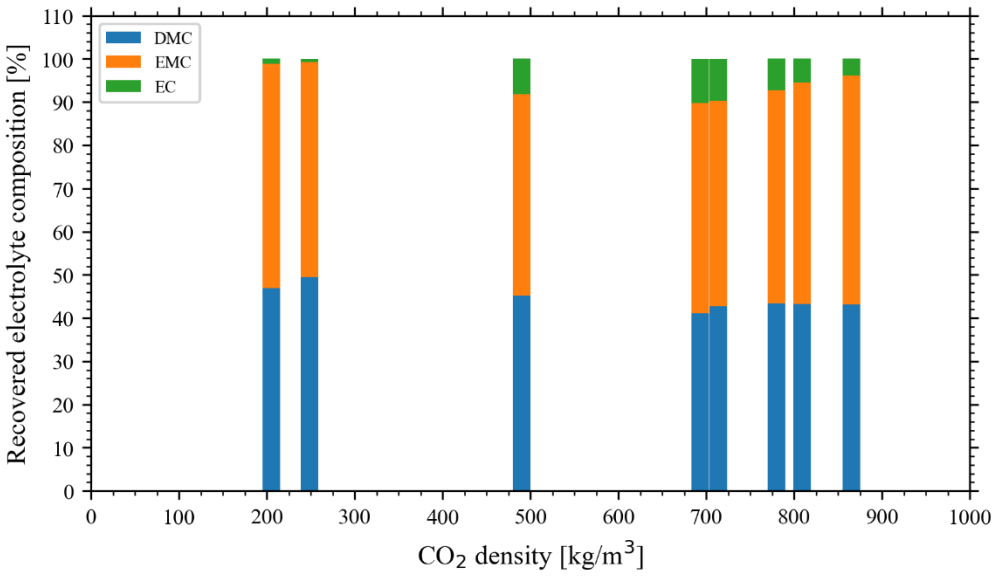

Figure 18. Composition of the collected liquid phase product obtained at various CO_2 process densities based on the GC-MS analysis.

ICP-OES was used to further determine the (metal) purity of the collected extract. Phosphorous (362±65 mg/L) and aluminum (5.2±0.4 mg/L) were detected at all process conditions, whereas the content of lithium was below the detection limit of the instrument.

The exhaust gas from the cold trap outlet was constantly analyzed with FTIR spectroscopy during the entire process time and the result for the process conditions resulting in a CO_2 density of 715 kg/m^3 is plotted in Figure 19a. The process conditions with a CO2 density of

715 kg/m^3 was selected, because it yields the highest electrolyte separation efficiency. Strong CO_2 vibration peaks (3728 cm^{-1}, 3704 cm^{-1}, 3624cm^{-1}, 3599 cm^{-1}, 2349 cm^{-1} (broad)) and weak peaks belonging to carbon monoxide (around 2075 cm^{-1}) were observed at all process times. Additionally, vibrational peaks associated with DMC (1780 cm^{-1} (νC=O), 1463 cm^{-1} (CH_3 sym. def.), and 1295 cm^{-1} (ν_aO-C-O)) and EMC (1772 cm^{-1} (νC=O), 1378 cm^{-1} (CH_3) and 1370 cm^{-1}) were detected. Vibrational peaks belonging to EC in gas phase (1876 cm^{-1}, 1868 cm^{-1}, and 1860 cm^{-1}) could not be observed. Moreover, vibrational peaks corresponding to $LiPF_6$ decomposition products HF (4000 cm^{-1} to 3600 cm^{-1}) and POF_3 (1428 cm^{-1}, 1416 cm^{-1}, 1404 cm^{-1} and 991 cm^{-1}) were not observed in the cold trap exhaust gas. The FTIR spectra of the exhaust gas emissions before the collection of the extract is plotted in Figure 19b. In addition to the vibrational peaks of DMC and EMC, characteristic peaks of EC were detected. Again, vibrational peaks corresponding to HF and POF_3 were not observed.

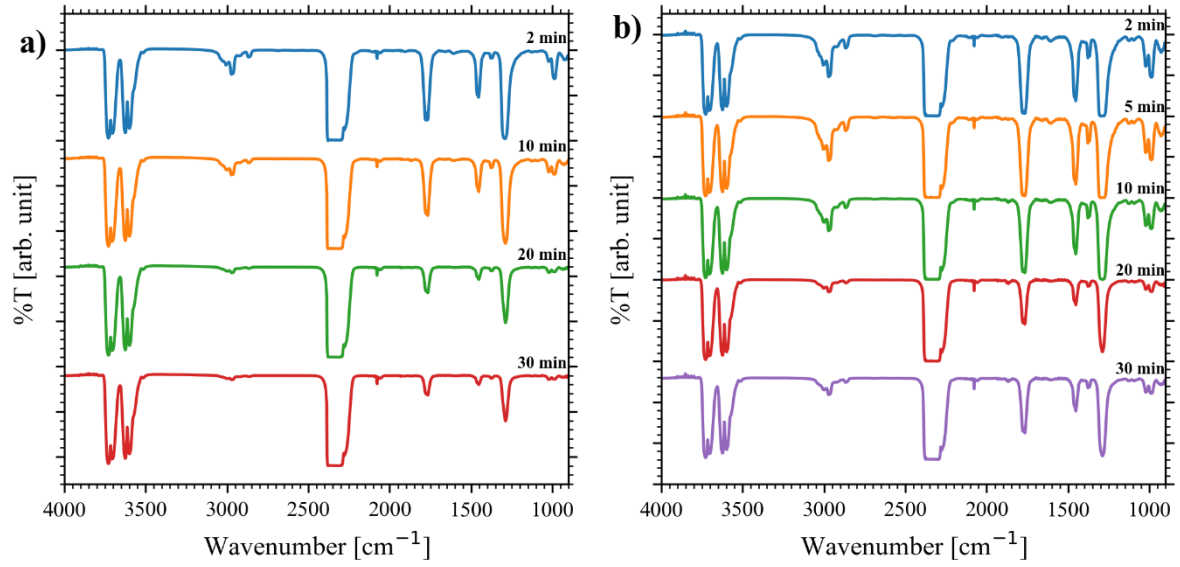

Figure 19. FTIR spectra of the process exhaust gas-emission at various process times with a CO_2 density of 715 kg/m^3 a) after and b) before the collection of the extract.

XRD analysis was used to determine the impact of the proposed extraction process on the active cathode material. In Figure 20 the XRD pattern of the active cathode material of an untreated sample and a sample treated at a CO_2 density of 810 kg/m^3, where high separation efficiency at the highest-pressure condition (120 bar) was observed, is plotted in the 2Θ range from 10º to 80º. The PDF card diffraction lines of NMC, and $LiMn_2O_4$ serve as a reference. The crystal structure of the cathode active material is unaffected by the subcritical CO_2 process. The diffraction peaks of both active cathode materials correspond to rhombohedral-structured NMC with a R-3m space group and cubic-structured lithium manganese oxide ($LiMnO_4$) with a Fd- 3m space group.

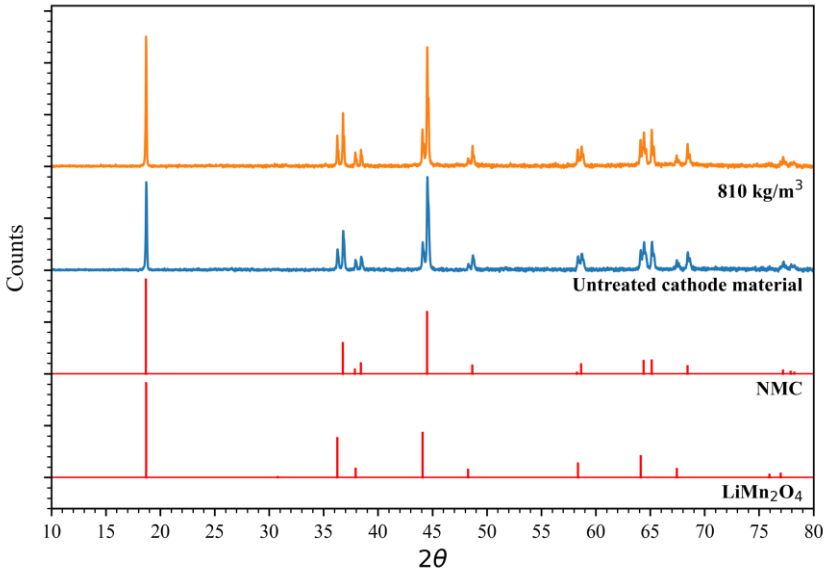

Figure 20. The XRD pattern of the active cathode material of an untreated sample and a sample treated at a CO_2 density of 810kg/m^3 in the 2Θ range from 10° to 80°. The PDF card diffraction pattern from NMC, and $LiMn_2O_4$ are plotted as a reference.

6. Discussion

This discussion chapter is divided into two parts according to results presented of the two processes; low temperature thermal treatment and sub-scCO_2 extraction process.

6.1. Low Temperature Thermal Treatment Process

In the low temperature thermal treatment process the weight loss of the electrode stack leveled off after 130ºC, reaching a weight loss of 13.9wt%. The separated electrolyte components by the low temperature thermal treatment process were subsequently recovered in solid and liquid phases. As ATR-FITR and XRD analysis show, most of the EC was recovered in solid phase, whereas GC-MS analysis of the liquid sample revealed that the liquid phase product was composed of DMC, EMC and minor amounts of EC. EC has a melting point of 36.5°C, whereas the melting points of DMC (4ºC) and EMC (-55ºC) are significantly lower, as shown in Table 1. The separated EC condensed on the walls of the quartz tube located outside of the heating zone of the tube furnace. By removing the quartz tube from the tube furnace, the quartz tube wall temperature dropped below the EC melting point, which led to the crystallization to monoclinic EC. The high melting point of EC enables the possibility to directly separate the electrolyte solvent EC from the other low melting point electrolyte solvents DMC and EMC. The electrolyte solvents (DMC, EMC, and EC) in the sample were successfully separated from the spent LiB electrode stack after the low temperature thermal treatment process at all process temperatures, as a disappearance of the DMC and EMC gas emission after 80 minutes at 130ºC and 150ºC was observed in the exhaust gas emission analysis. It is reported in the literature that the electrolyte solvents DMC, EMC and EC eventually decompose to CO_2, carbon monoxide (CO), ethene (C_2H_4), and dimethyl ether (C_2H_6O) at temperatures above 180ºC [84]. However, in the process exhaust gas at various temperature conditions, characteristic vibrational peaks associated with CO_2, CO, C_2H_4, and C_2H_6O were not detected. This is proof that DMC, EMC and EC did not degrade during the low temperature thermal treatment process and were successfully recovered as solid and liquid phase products.

While the electrolyte solvents were successfully recovered, $LiPF_6$ decomposed in the process at all temperatures into gaseous HF and POF_3 as stated in equations 2 and 3, as their presence was detected in the process exhaust gas. The anhydrous $LiPF_6$ decomposition product PF_5 (Eq. 1) was challenging to identify in the process exhaust gas with high certainty due to the overlap of the characteristic vibrational peaks of PF_5 at 1018cm^{-1} and 946cm^{-1} with the vibrational peaks of the organic solvents [39]. However, the formation of PF_5 during the low temperature thermal treatment should not be ruled out. Whereas POF_3 peaks were still present in the exhaust gas after the entire process time at 90ºC and 110ºC, the POF_3 peaks levelled off after 70 minutes at 130ºC and 150ºC. This is evidence that $LiPF_6$, fully decomposed to HF and POF_3 at process temperature conditions above 130ºC but did not entirely degrade at 90ºC and 110ºC. This finding is in alignment with recent studies in which a weight percentage drop of $LiPF_6$ to 17wt%, the proportion of LiF, at temperatures up to 150ºC was observed in TGA measurement [83]. It was noticeable that with the increase in temperature, the standard deviation of the triplicates decreased. The deviation in the weight loss can be associated with the incomplete degradation of $LiPF_6$ at process temperatures below 130ºC. The moisture/humidity responsible for the hydrolysis composition (Eq. 3) of $LiPF_6$ was believed to be absorbed into the LiB sample during the cell disassembly, the sample preparation process, and the cell storage at -18ºC.

A secure exhaust treatment system is essential for the proposed low temperature thermal treatment process due to the release of the toxic gases HF and POF_3. The presence of F^- and PO_4^{3-} in the gas washing water is evidence that hydrofluoric acid and phosphoric acid were formed after the reaction of HF and POF_3 with H_2O as stated in equations 2 and 3. Hydrofluoric acid and phosphoric acid can be considered as process by-products and potentially reutilized. However, more investigation is required.

While keeping in mind the complete $LiPF_6$ degradation duration of 70 minutes at 130ºC, the disappearance of the DMC and EMC gas emission after 80 minutes, as well as the energy efficiency of the process, the efficient process time to separate and recover the electrolyte from the spent LiB sample was determined to be 80 minutes.

6.2. Sub- and Supercritical CO_2 Extraction Process

The CO_2 density is the driving force for the electrolyte component extraction from the spent LiB electrolyte stack. Steady separation efficiency of 66% with respect to the standard deviations was observed at CO_2 densities between 600-900 kg/m^3. GC-MS analysis of the collected liquid extract revealed DMC and EMC as the main constituents, with minor amounts of EC (<10%). The extract collection efficiency in the process was around 60% and the analysis of the cold trap exhaust gas revealed the inefficient collection of DMC and EMC. However, the EC collection efficiency was believed to be high due to the absence of the vibrational peaks in the cold trap exhaust gas. Thus, the quantification of the collected extract was not representative of the actual share of extracted electrolyte solvent, leading to an overestimation of the EC extraction efficiency.

$ScCO_2$ is known to be a good solvent for non-polar low molecular weight compounds. DMC and EMC are linear carbonates with a low dielectric constant and dipole moment compared to the cyclic EC. Thus, the electrolyte components DMC and EMC could be selectively separated with high efficiencies from the spent LiB battery waste using pure sub-$scCO_2$ at densities between 600-900 kg/m^3, while the polar electrolyte component EC was only partly separated in the process.

The analysis of the process exhaust gas indicated also that $LiPF_6$ did not decompose during the process since HF and POF_3 vibrational peaks were not observed. The detected amount of phosphorous in the collected extract corresponded to only a trace amount of $LiPF_6$ (<1.2%) estimated based on a $LiPF_6$ concentration of 1 M. It is believed that the phosphorous originated from electrolyte aging products such as DMFP and EMFP, which were detected in the GC-MS analysis. Accordingly, the proposed process eliminated the toxic-gas emission originating from the decomposition of the thermal-unstable $LiPF_6$.

In the proposed process, the polar electrolyte components, EC and $LiPF_6$, precipitated and are assumed to be left as a residue in the sample, which explains the low electrolyte separation efficiency of 66%. An additional extraction step for the recovery of the precipitated polar electrolyte components, EC and $LiPF_6$ is required. The solvation characteristics of $scCO_2$ can be significantly improved with the addition of a co-solvent or a modifier. An increase in the extraction efficiency of EC and $LiPF_6$ with the use of an aprotic co-solvent has been reported by Grützke et al., [24].

The crystal structure of the cathode active material was unaffected by the subcritical CO_2 process using the highest-pressure condition of 120 bar. It can be concluded that the proposed process has no impact on the cathode active material composition and crystal structure, which means that subsequent state-of-the-art recovery methods for the valuable active materials are unaffected by the sub- and scCO_2 electrolyte solvent extraction process.

7. Conclusions

The low temperature thermal treatment approach enabled the separation and collection of the electrolyte solvents DMC, EMC, and EC from the spent LiB after 80 minutes at 130ºC under constant N_2 flow. Analysis of the process exhaust gas revealed that $LiPF_6$ was not recovered intact, as it decomposed at all investigated process conditions. Instead, the toxic gaseous decomposition products HF and POF_3 were separated from the sample and their acids were obtained by exhaust washing treatment, whereas the solid LiF remained in the sample. The separated electrolyte solvents were collected as solid and liquid phases. The solid phase product was composed of monoclinic EC with elemental impurities of Li (0.8 ppm), Mn (2.3 ppm), Co (0.94 ppm), Cu (1.29 ppm), Ni (0.57 ppm), and Al (0.16 ppm). The liquid phase product was composed of the electrolyte solvents DMC, EMC and minor amounts of EC. The electrolyte separation efficiency in the process was estimated to be 98% with effective recovery of organic solvents but sacrificing $LiPF_6$.

A lower electrolyte separation efficiency of 66% was obtained in the sub-$scCO_2$ extraction process at CO_2 densities between 600-900 kg/m^3 after 30 minutes because the process was suitable to separate the non-polar electrolyte solvents DMC and EMC efficiently from the spent LiB. Apart from achieving high recycling efficiencies, the electrolyte separation process is relatively safe for workers in the recycling plant and must have a minimized impact on the environment. The exhaust gas analysis and elemental analysis of the collected extract indicated that $LiPF_6$ did not decompose during the process but remained intact in the spent LiB. Apart from DMC, EMC, and minor amounts of EC, traces of the electrolyte aging products DEC, DMFP, EMFP, and the electrolyte additive VC were detected in the collected extracts. Furthermore, elemental analysis showed P (362±65 mg/L) and Al (5.2±0.4 mg/L) as impurities, whereas P, whose detected amount corresponded to only a trace amount of $LiPF_6$ (<1.2% of 1 M $LiPF_6$) was believed to originate from electrolyte aging products. XRD analysis revealed that the active cathode material was unaffected by the subcritical CO_2 extraction process with the highest-pressure condition of 120 bar.

$ScCO_2$ extraction is a promising process to recover the electrolyte, non-polar and polar components, with minimal toxic-gas emission but further research is needed to understand the extraction system and the behavior of the polar electrolyte components.

8. Future Work

In this work two different approaches to recycle the electrolyte from spent LiB were studied and compared. The sub-sc-CO_2 extraction process is promising due to its toxic-free gas emissions. However, the polar electrolyte solvent EC and the conductive salt $LiPF_6$ were not successfully recovered. It is believed that the polar electrolyte components can be recycled with co-solvent modified scCO_2 extraction. For a high selective extraction of the polar electrolyte components a thorough investigation using a suitable co-solvent and the optimal process conditions (pressure, temperature, density, flow-rate, and extraction time) is required.

After the development of the successful extraction of the polar electrolyte components, the process must be tested on various spent LiB samples with different cell chemistries and electrolyte formulations.

Extensive analysis of the purity of the extracted product must be performed before its reutilization in the industry. If necessary, purification techniques must be investigated to achieve battery-grade electrolyte solvents and conductive salt.

Acknowledgments

First, I would like to express my deepest gratitude to Burçak Ebin, my supervisor, for your mentorship, guidance, support, feedback, openness for discussions of all sorts and everyhting you taught me since the beginning.

I am extremely grateful to Marina Petranikova, my co-supervisor, for your feedback to all my work, your moral support, motivation boosts, and open-door-police with all kinds of questions to share of your expertise.

Many thanks to Christian Ekberg for all your feedback and sound critics throughout the writing process.

Big thanks to my past and present co-workers at NC/IMR, seniors and PhDs, for providing an excellent work environment, your help and expertise, and innumerable amount of fikas and after works.

I could not have undertaken this journey without my friends based in Gothenburg, Sweden, Germany and the rest of the world. I am certain you know, who I am referring to. Thank you for your moral support, providing distraction, broaden continually my horizon, and all the adventures and memories we share.

Last but not least, I am deeply grateful to my family for your unlimited love and support.

This work was supported by the Swedish Energy Agency Battery Fund Program (Project No:50124-10) and by FORMAS – Swedish Research Council for Sustainable Development (Project No: 2021-01699).

References.

[1] N. Nitta, F. Wu, J.T. Lee, G. Yushin, Li-ion battery materials: Present and future, Mater. Today. 18 252–264. https://doi.org/10.1016/j.mattod.2014.10.040.

[2] J.M. Tarascon, M. Armand, Issues and challenges facing rechargeable lithium batteries, Nature. 414 (2001) 359–367. https://doi.org/10.1038/35104644.

[3] G. Harper, R. Sommerville, E. Kendrick, L. Driscoll, P. Slater, R. Stolkin, A. Walton, P. Christensen, O. Heidrich, S. Lambert, A. Abbott, K. Ryder, L. Gaines, P. Anderson, Recycling lithium-ion batteries from electric vehicles, Nature. 575 (2019) 75–86. https://doi.org/10.1038/s41586-019-1682-5.

[4] M. Romare, L. Dahllöf, The Life Cycle Energy Consumption and Greenhouse Gas Emissions from Lithium-Ion Batteries A study with focus on Current Technology and batteries for ligh-duty vehicles., 2017. http://www.ivl.se/download/18.5922281715bdaebede9559/1496046218976/C243+The+life+cycle+energy+consumption+and+CO2+emissions+from+lithium+ion+batteries+.pdf.

[5] D.L. Thompson, J.M. Hartley, S.M. Lambert, M. Shiref, G.D.J. Harper, E. Kendrick, P. Anderson, K.S. Ryder, L. Gaines, A.P. Abbott, The importance of design in lithium ion battery recycling-a critical review, Green Chem. 22 (2020) 7585–7603. https://doi.org/10.1039/d0gc02745f.

[6] Global EV Outlook 2020, OECD, 2020. https://doi.org/10.1787/d394399e-en.

[7] Global EV Outlook 2022, OECD, 2022. https://doi.org/10.1787/c83f815c-en.

[8] L. Usai, J.J. Lamb, E. Hertwich, O.S. Burheim, A.H. Strømman, Analysis of the Li-ion battery industry in light of the global transition to electric passenger light duty vehicles until 2050, Environ. Res. Infrastruct. Sustain. 2 (2022) 011002. https://doi.org/10.1088/2634-4505/ac49a0.

[9] J. Neumann, M. Petranikova, M. Meeus, J.D. Gamarra, R. Younesi, M. Winter, S. Nowak, Recycling of Lithium-Ion Batteries — Current State of the Art , Circular Economy , and Next Generation Recycling, 2102917 (2022). https://doi.org/10.1002/aenm.202102917.

[10] A. Sobianowska-Turek, W. Urbańska, A. Janicka, M. Zawiślak, J. Matla, The Necessity of Recycling of Waste Li-Ion Batteries Used in Electric Vehicles as Objects Posing a Threat to Human Health and the Environment, Recycling. 6 (2021) 35. https://doi.org/10.3390/recycling6020035.

[11] N.P. Lebedeva, L. Boon-Brett, Considerations on the Chemical Toxicity of Contemporary Li-Ion Battery Electrolytes and Their Components, J. Electrochem. Soc. 163 (2016) A821–A830. https://doi.org/10.1149/2.0171606jes.

[12] A. Nedjalkov, J. Meyer, M. Köhring, A. Doering, M. Angelmahr, S. Dahle, A. Sander, A. Fischer, W. Schade, Toxic Gas Emissions from Damaged Lithium Ion Batteries—Analysis and Safety Enhancement Solution, Batteries. 2 (2016) 5. https://doi.org/10.3390/batteries2010005.

[13] F. Larsson, P. Andersson, P. Blomqvist, B.E. Mellander, Toxic fluoride gas emissions from lithium-ion battery fires, Sci. Rep. 7 (2017) 1–13. https://doi.org/10.1038/s41598-017-09784-z.

[14] P. Andersson, P. Blomqvist, A. Lorén, F. Larsson, Investigation of fire emissions from Li-ion batteries, n.d.

[15] F. Arshad, L. Li, K. Amin, E. Fan, N. Manurkar, A. Ahmad, J. Yang, F. Wu, R. Chen, A Comprehensive Review of Advancement in Recycling Anode and Electrolyte from Spent Lithium Ion Batteries, ACS Sustain. Chem. Eng. 8 (2020) 13527–13554. https://doi.org/10.1021/acssuschemeng.0c04940.

[16] J.A. Kinnaird, P.A.M. Nex, Critical raw materials, Routledge Handb. Extr. Ind. Sustain. Dev. (2022) 13–33. https://doi.org/10.4324/9781003001317-3.

[17] Business Sweden, The Nordic Battery Value Chain, (2023).

[18] T. McPhie, A. Parrondo Crespo, Zero emission vehicles: first 'Fit for 55'' deal will end the sale of new CO2 emitting cars in Europe by 2035,' Eur. Comm. (2022) 6462. https://ec.europa.eu/commission/presscorner/detail/en/IP_22_6462.

[19] EUR-Lex, Directive 2006/66/EC of the European Parliament and of the Council of 6 September 2006 on batteries and accumulators and waste batteries and accumulators and repealing Directive 91/157/EEC, Off. J. Eur. Union. L 266 (2006) 1–14.

[20] Regulation of the European Parliament and of the Council concerning batteries and waste batteries, repealing. Directive 2006/66/EC and amending Regulation (EU) No 2019/1020, Eur. Comm. 0353 (2020). https://eur-lex.europa.eu/legal-content/EN/TXT/?uri=CELEX%3A52020PC0798.

[21] Commission of the European Communities (EC), ANNEXES to the Proposal for a Regulation of the European Parliament and of the Council concerning batteries and waste batteries, repealing Directive 2006/66/EC and amending Regulation (EU) No 2019/1020, 4 (2020) 1–23.

[22] C. Ekberg, M. Petranikova, Lithium Batteries Recycling, in: Lithium Process Chem. Resour. Extr. Batter. Recycl., Elsevier Inc., 2015: pp. 233–267. https://doi.org/10.1016/B978-0-12-801417-2.00007-4.

[23] J. Marshall, D. Gastol, R. Sommerville, B. Middleton, V. Goodship, E. Kendrick, Disassembly of Li Ion Cells—Characterization and Safety Considerations of a Recycling Scheme, Metals (Basel). 10 (2020) 773. https://doi.org/10.3390/met10060773.

[24] D. Thompson, C. Hyde, J.M. Hartley, A.P. Abbott, P.A. Anderson, G.D.J. Harper, To shred or not to shred: A comparative techno-economic assessment of lithium ion battery hydrometallurgical recycling retaining value and improving circularity in LIB supply chains, Resour. Conserv. Recycl. 175 (2021) 105741. https://doi.org/10.1016/j.resconrec.2021.105741.

[25] F. Diaz, Y. Wang, R. Weyhe, B. Friedrich, Gas generation measurement and evaluation during mechanical processing and thermal treatment of spent Li-ion batteries, Waste Manag. 84 (2019) 102–111. https://doi.org/10.1016/j.wasman.2018.11.029.

[26] R. Zhang, X. Shi, O.C. Esan, L. An, Organic Electrolytes Recycling From Spent Lithium-Ion Batteries, Glob. Challenges. (2022) 2200050. https://doi.org/10.1002/gch2.202200050.

[27] S. Nowak, M. Winter, The role of sub- and supercritical CO2 as "processing solvent" for the recycling and sample preparation of lithium ion battery electrolytes, Molecules. 22 (2017). https://doi.org/10.3390/molecules22030403.

[28] E. Mossali, N. Picone, L. Gentilini, O. Rodrìguez, J.M. Pérez, M. Colledani, Lithium-ion batteries towards circular economy: A literature review of opportunities and issues of recycling treatments, J. Environ. Manage. 264 (2020) 110500. https://doi.org/10.1016/j.jenvman.2020.110500.

[29] V. PEM TWTH Aachen, PRODUCTION PROCESS OF A LITHIUM-ION BATTERY CELL, (2023).

[30] J. Choi, P.J. Kim, A roadmap of battery separator development: Past and future, Curr. Opin. Electrochem. 31 (2022) 100858. https://doi.org/10.1016/j.coelec.2021.100858.

[31] M. Li, C. Wang, Z. Chen, K. Xu, J. Lu, New Concepts in Electrolytes, Chem. Rev. 120 (2020) 6783–6819. https://doi.org/10.1021/acs.chemrev.9b00531.

[32] Y. Horowitz, C. Schmidt, D. Yoon, L.M. Riegger, L. Katzenmeier, G.M. Bosch, M. Noked, Y. Ein-Eli, J. Janek, W.G. Zeier, C.E. Diesendruck, D. Golodnitsky, Between Liquid and All Solid: A Prospect on Electrolyte Future in Lithium-Ion Batteries for Electric Vehicles, Energy Technol. 8 (2020) 2000580. https://doi.org/10.1002/ente.202000580.

[33] K. Xu, Li-ion battery electrolytes, Nat. Energy. 6 (2021) 763. https://doi.org/10.1038/s41560-021-00841-6.

[34] K. Xu, Nonaqueous liquid electrolytes for lithium-based rechargeable batteries, Chem. Rev. 104 (2004) 4303–4417. https://doi.org/10.1021/cr030203g.

[35] D. Hubble, D.E. Brown, Y. Zhao, C. Fang, J. Lau, B.D. McCloskey, G. Liu, Liquid electrolyte development for low-temperature lithium-ion batteries, Energy Environ. Sci. 15 (2022) 550–578. https://doi.org/10.1039/d1ee01789f.

[36] K. Xu, Nonaqueous liquid electrolytes for lithium-based rechargeable batteries, Chem. Rev. 104 (2004) 4303–4417. https://doi.org/10.1021/cr030203g.

[37] European Commission, EU 1272/2008 – Classification, Labelling and Packaging of Substances and Mixtures, Med. Device Guidel. Regul. Handb. (2022) 261–295. https://doi.org/10.1007/978-3-030-91855-2_14.

[38] S. Bertilsson, F. Larsson, M. Furlani, I. Albinsson, B.E. Mellander, Lithium-ion battery electrolyte emissions analyzed by coupled thermogravimetric/Fourier-transform infrared spectroscopy, J. Power Sources. 365 (2017) 446–455. https://doi.org/10.1016/j.jpowsour.2017.08.082.

[39] H. Yang, G. V. Zhuang, P.N. Ross, Thermal stability of LiPF6 salt and Li-ion battery electrolytes containing LiPF6, J. Power Sources. 161 (2006) 573–579. https://doi.org/10.1016/j.jpowsour.2006.03.058.

[40] P. Andersson, P. Blomqvist, A. Lorén, F. Larsson, Using Fourier transform infrared spectroscopy to determine toxic gases in fires with lithium-ion batteries, Fire Mater. 40 (2016) 999–1015. https://doi.org/10.1002/fam.2359.

[41] L.D. Kock, M.D.S. Lekgoathi, P.L. Crouse, B.M. Vilakazi, Solid state vibrational spectroscopy of anhydrous lithium hexafluorophosphate (LiPF 6), J. Mol. Struct. 1026 (2012) 145–149. https://doi.org/10.1016/j.molstruc.2012.05.053.

[42] B. Ravdel, K.M. Abraham, R. Gitzendanner, J. DiCarlo, B. Lucht, C. Campion, Thermal stability of lithium-ion battery electrolytes, in: J. Power Sources, Elsevier, 2003: pp. 805–810. https://doi.org/10.1016/S0378-7753(03)00257-X.

[43] X.G. Teng, F.Q. Li, P.H. Ma, Q. Du Ren, S.Y. Li, Study on thermal decomposition of lithium hexafluorophosphate by TG-FT-IR coupling method, Thermochim. Acta. 436 (2005) 30–34. https://doi.org/10.1016/j.tca.2005.07.004.

[44] S. Vanderburgt, R.M. Santos, Y.W. Chiang, Is it worthwhile to recover lithium-ion battery electrolyte during lithium-ion battery recycling?, Resour. Conserv. Recycl. 189 (2023) 106733. https://doi.org/10.1016/j.resconrec.2022.106733.

[45] S. Nowak, M. Winter, The Role of Sub- and Supercritical CO2 as “Processing Solvent” for the Recycling and Sample Preparation of Lithium Ion Battery Electrolytes, Molecules. 22 (2017) 403. https://doi.org/10.3390/molecules22030403.

[46] X. Zhong, W. Liu, J. Han, F. Jiao, W. Qin, T. Liu, C. Zhao, Pyrolysis and physical separation for the recovery of spent LiFePO 4 batteries, Waste Manag. 89 (2019) 83–93. https://doi.org/10.1016/j.wasman.2019.03.068.

[47] F. Stehmann, C. Bradtmöller, S. Scholl, Separation of the Electrolyte—Thermal Drying, in: Sustain. Prod. Life Cycle Eng. Manag., Springer, 2018: pp. 139–153. https://doi.org/10.1007/978-3-319-70572-9_8.

[48] Umweltfreundliches Recycling von Lithium-Ionen-Batterien., (n.d.). https://www.duesenfeld.com/index_de.html (accessed February 8, 2023).

[49] S. Lei, W. Sun, Y. Yang, Solvent extraction for recycling of spent lithium-ion batteries, J. Hazard. Mater. (2021) 127654. https://doi.org/10.1016/j.jhazmat.2021.127654.

[50] K. He, Z.Y. Zhang, L. Alai, F.S. Zhang, A green process for exfoliating electrode materials and simultaneously extracting electrolyte from spent lithium-ion batteries, J. Hazard. Mater. 375 (2019) 43–51. https://doi.org/10.1016/j.jhazmat.2019.03.120.

[51] Y. Zhu, Q. Ding, Y. Zhao, J. Ai, Y. Li, Y.C. Cao, Study on the process of harmless treatment

of residual electrolyte in battery disassembly, Waste Manag. Res. 38 (2020) 1295–1300. https://doi.org/10.1177/0734242X20914752.

[52] P. Haas, S. Pfeifer, J. Müller, C. Bradtmöller, S. Scholl, Separation of the Electrolyte—Solvent Extraction, in: Sustain. Prod. Life Cycle Eng. Manag., Springer, 2018: pp. 155–176. https://doi.org/10.1007/978-3-319-70572-9_9.

[53] S. Lee, Green chemistry and chemical engineering, Part. Technol. Appl. (2016) vii–viii. https://doi.org/10.1007/978-1-4939-9060-3.

[54] K. Shanab, C. Neudorfer, E. Schirmer, H. Spreitzer, Green Solvents in Organic Synthesis: An Overview, Curr. Org. Chem. 17 (2013) 1179–1187. https://doi.org/10.2174/1385272811317110005.

[55] L.S. Daintree, A. Kordikowski, P. York, Separation processes for organic molecules using SCF Technologies, Adv. Drug Deliv. Rev. 60 (2008) 351–372. https://doi.org/10.1016/j.addr.2007.03.024.

[56] S.P. Nalawade, F. Picchioni, L.P.B.M. Janssen, Supercritical carbon dioxide as a green solvent for processing polymer melts: Processing aspects and applications, Prog. Polym. Sci. 31 (2006) 19–43. https://doi.org/10.1016/j.progpolymsci.2005.08.002.

[57] P. Raveendran, Y. Ikushima, S.L. Wallen, Polar attributes of supercritical carbon dioxide, Acc. Chem. Res. 38 (2005) 478–485. https://doi.org/10.1021/ar040082m.

[58] M.D.L. de Castro, M. Valcárcel, M.T. Tena, Analytical Supercritical Fluid Extraction, Springer Berlin Heidelberg, 1994. https://doi.org/10.1007/978-3-642-78673-0.

[59] M. Grützke, V. Kraft, W. Weber, C. Wendt, A. Friesen, S. Klamor, M. Winter, S. Nowak, Supercritical carbon dioxide extraction of lithium-ion battery electrolytes, J. Supercrit. Fluids. 94 (2014) 216–222. https://doi.org/10.1016/j.supflu.2014.07.014.

[60] M. Grützke, X. Mönnighoff, F. Horsthemke, V. Kraft, M. Winter, S. Nowak, Extraction of lithium-ion battery electrolytes with liquid and supercritical carbon dioxide and additional solvents, RSC Adv. 5 (2015) 43209–43217. https://doi.org/10.1039/c5ra04451k.

[61] Y. Liu, D. Mu, R. Zheng, C. Dai, Supercritical CO2 extraction of organic carbonate-based electrolytes of lithium-ion batteries, RSC Adv. 4 (2014) 54525–54531. https://doi.org/10.1039/c4ra10530c.

[62] Y. Liu, D. Mu, Y. Dai, Q. Ma, R. Zheng, C. Dai, Analysis on Extraction Behaviour of Lithium-ion Battery Electrolyte Solvents in Supercritical CO 2 by Gas Chromatography, Int. J. Electrochem. Sci. 11 (2016) 7594–7604. https://doi.org/10.20964/2016.09.03.

[63] Y. Liu, D. Mu, R. Li, Q. Ma, R. Zheng, C. Dai, Purification and Characterization of Reclaimed Electrolytes from Spent Lithium-Ion Batteries, J. Phys. Chem. C. 121 (2017) 4181–4187. https://doi.org/10.1021/acs.jpcc.6b12970.

[64] X. Mönnighoff, A. Friesen, B. Konersmann, F. Horsthemke, M. Grützke, M. Winter, S. Nowak, Supercritical carbon dioxide extraction of electrolyte from spent lithium ion batteries and its characterization by gas chromatography with chemical ionization, J. Power Sources. 352 (2017) 56–63. https://doi.org/10.1016/j.jpowsour.2017.03.114.

[65] D. Mu, Y. Liu, R. Li, Q. Ma, C. Dai, Transcritical CO2 extraction of electrolytes for lithium-ion batteries: Optimization of the recycling process and quality-quantity variation, New J. Chem. 41 (2017) 7177–7185. https://doi.org/10.1039/c7nj00771j.

[66] S. Sloop, L. Crandon, M. Allen, K. Koetje, L. Reed, L. Gaines, W. Sirisaksoontorn, M. Lerner, A direct recycling case study from a lithium-ion battery recall, Sustain. Mater. Technol. 25 (2020) e00152. https://doi.org/10.1016/j.susmat.2020.e00152.

[67] G. Harper, P.A. Anderson, E. Kendrick, W. Mrozik, P. Christensen, S. Lambert, D. Greenwood, P.K. Das, M. Ahmeid, Z. Milojevic, W. Du, D.J.L. Brett, P.R. Shearing, A. Rastegarpanah, R. Solkin, R. Sommerville, A. Zorin, J.L. Durham, A. Abbott, D. Thompson, N. Browning, L. Mehdi, M. Bahri, F. Schnaider-Tontini, D. Nicholls, C. Stallmeister, B. Friedrich, M. Sommerfeld, L.L. Driscoll, A. Jarvis, E.C. Giles, P.R. Slater, V. Echavarri-

Bravo, G. Maddalena, L. Horsfall, L. Gaines, Q. Dai, S.J. Jethwa, A.L. Lipson, G.A. Leeke, T.D. Cowell, J.G. Farthing, G. Mariani, A. Smith, Z. Iqbal, R. Golmohammadzadeh, L. Sweeney, V. Goodship, Z. Li, J.S. Edge, L. Lander, V. Nguyen-Tien, R.J.R. Elliott, O. Heidrich, M. Slattery, D. Reed, J. Ahuja, A. Cavoski, R. Lee, E. Driscoll, J. Baker, P.B. Littlewood, I. Styles, S. Mahanty, F. Boons, Roadmap for a sustainable circular economy in lithium-ion and future battery technologies, J. Phys. Energy. 5 (2022) 021501. https://doi.org/10.1088/2515-7655/acaa57.

[68] D.M. Werner, T. Mütze, U.A. Peuker, Influence of Cell Opening Methods on Electrolyte Removal during Processing in Lithium-Ion Battery Recycling, Metals (Basel). 12 (2022) 663. https://doi.org/10.3390/met12040663.

[69] J. Henschel, J.L. Schwarz, F. Glorius, M. Winter, S. Nowak, Further insights into structural diversity of phosphorus-based decomposition products in lithium ion battery electrolytes via liquid chromatographic techniques hyphenated to ion trap-time-of-flight mass spectrometry, Anal. Chem. 91 (2019) 3980–3988. https://doi.org/10.1021/acs.analchem.8b05229.

[70] W. Weber, V. Kraft, M. Grützke, R. Wagner, M. Winter, S. Nowak, Identification of alkylated phosphates by gas chromatography-mass spectrometric investigations with different ionization principles of a thermally aged commercial lithium ion battery electrolyte, J. Chromatogr. A. 1394 (2015) 128–136. https://doi.org/10.1016/j.chroma.2015.03.048.

[71] P. Raveendran, Y. Ikushima, S.L. Wallen, Polar attributes of supercritical carbon dioxide, Acc. Chem. Res. 38 (2005) 478–485. https://doi.org/10.1021/ar040082m.

[72] M. Altarsha, F. Ingrosso, M.F. Ruiz-Lopez, A New Glimpse into the CO_2 -Philicity of Carbonyl Compounds, ChemPhysChem. 13 (2012) 3397–3403. https://doi.org/10.1002/cphc.201200135.

[73] H.J. Vandenburg, A.A. Clifford, K.D. Bartle, J. Carroll, I. Newton, L.M. Garden, J.R. Dean, C.T. Costley, Analytical extraction of additives from polymers, Analyst. 122 (1997) 101R-116R. https://doi.org/10.1039/a704052k.

[74] Y. Fu, J. Schuster, M. Petranikova, B. Ebin, Innovative recycling of organic binders from electric vehicle lithium-ion batteries by supercritical carbon dioxide extraction, Resour. Conserv. Recycl. 172 (2021) 105666. https://doi.org/10.1016/j.resconrec.2021.105666.

[75] S. Shimizu, S. Abbott, How Entrainers Enhance Solubility in Supercritical Carbon Dioxide, J. Phys. Chem. B. 120 (2016) 3713–3723. https://doi.org/10.1021/acs.jpcb.6b01380.

[76] F.P. Lucien, N.R. Foster, Solubilities of solid mixtures in supercritical carbon dioxide: A review, J. Supercrit. Fluids. 17 (2000) 111–134. https://doi.org/10.1016/S0896-8446(99)00048-0.

[77] F. Ingrosso, M.F. Ruiz-López, Modeling Solvation in Supercritical CO2, ChemPhysChem. 18 (2017) 2560–2572. https://doi.org/10.1002/cphc.201700434.

[78] K.D. Bartle, T. Boddington, A.A. Clifford, S.B. Hawthorne, The Effect of solubility on the kinetics of dynamic supercritical-fluid extraction, J. Supercrit. Fluids. 5 (1992) 207–212. https://doi.org/10.1016/0896-8446(92)90009-9.

[79] S.F. Lux, I.T. Lucas, E. Pollak, S. Passerini, M. Winter, R. Kostecki, The mechanism of HF formation in LiPF6 based organic carbonate electrolytes, Electrochem. Commun. 14 (2012) 47–50. https://doi.org/10.1016/j.elecom.2011.10.026.

[80] V. Kraft, M. Grützke, W. Weber, M. Winter, S. Nowak, Ion chromatography electrospray ionization mass spectrometry method development and investigation of lithium hexafluorophosphate-based organic electrolytes and their thermal decomposition products, J. Chromatogr. A. 1354 (2014) 92–100. https://doi.org/10.1016/j.chroma.2014.05.066.

[81] H. Bohets, B.J. Van Der Veken, On the conformational behavior of dimethyl carbonate, Phys. Chem. Chem. Phys. 1 (1999) 1817–1826. https://doi.org/10.1039/a901046g.

[82] A.K. Das, K. Sunanda, B.N. Rajasekhar, Electronic and vibrational spectroscopy of ethyl methyl carbonate: A comparative experimental and theoretical study, J. Quant. Spectrosc.

Radiat. Transf. 272 (2021) 107789. https://doi.org/10.1016/j.jqsrt.2021.107789.

[83] B. Fortunato, P. Mirone, G. Fini, Infrared and Raman spectra and vibrational assignment of ethylene carbonate, Spectrochim. Acta Part A Mol. Spectrosc. 27 (1971) 1917–1927. https://doi.org/10.1016/0584-8539(71)80245-3.

[84] Z. Liao, S. Zhang, Y. Zhao, Z. Qiu, K. Li, D. Han, G. Zhang, T.G. Habetler, Experimental evaluation of thermolysis-driven gas emissions from LiPF6-carbonate electrolyte used in lithium-ion batteries, J. Energy Chem. 49 (2020) 124–135. https://doi.org/10.1016/j.jechem.2020.01.030.